MASTERARBEIT | MASTER'S THESIS

Titel | Title

Testing the amphiphilic character of poly(acrylamide-co-styrene)

verfasst von | submitted by

Jana Schöffmann BSc BSc

angestrebter akademischer Grad | in partial fulfilment of the requirements for the degree of

Diplom-Ingenieurin (Dipl.-Ing.)

Wien | Vienna, 2025

Studienkennzahl lt. Studienblatt | Degree programme code as it appears on the student record sheet:	UA 066 658
Studienrichtung lt. Studienblatt | Degree programme as it appears on the student record sheet:	Masterstudium Chemie und Technologie der Materialien
Betreut von | Supervisor:	Univ.-Prof. Dr. Alexander Bismarck

First, I would like to thank my supervisor, Alexander Bismarck, for giving me the amazing opportunity to perform my research in his group and for all his support. I would also like to thank my co-supervisor Emina Muratspahic, who provided invaluable support during my practical work. I am grateful for our cooperation and proud of what we have achieved together. I also want to thank all members of the PaCE group who supported me during my time in the group.

I would like to thank my parents Gabriele and Michael and my brother Leo, who have supported me tirelessly during my studies, not only financially but also emotionally. Last but not least, I would like to thank Christoph. You have always encouraged me to be the best version of myself.

Table of Contents

Abbreviations

DRAs ... Drag-reducing agents

PAM ... Polyacrylamide

CTAB ... cetyltrimethylammonium bromide

HEMA ... 2-hydroxyethyl methacrylate

MBAm ... N,N-methylenebisacrylamide

TEMED ... N,N,N',N'-tetramethyl ethylenediamine

GPC ... Gel permeation chromatography

ViEDRA ... Vienna Experiment for Drag Reducing Agents

SEM ... Scanning electron microscopy

V_h ... hydrodynamic volume

1 Introduction

1.1 Copolymers of Amphiphilic Nature and Macrosurfactants

The demand for polymers is at an all-time high. The development of functional polymers is of particular interest, as they can have a significant impact in many fields, including the medical and pharmaceutical industry, the oil and gas industry, and water treatment.[1] Polymers can be classified into two categories: homopolymers and copolymers. Copolymers, in turn, can be further subdivided into three distinct types: alternating, statistical, and block copolymers. In block copolymers, the monomers are discrete entities that appear along the polymer backbone. The architecture of block copolymers is not constrained; they can be branched, linear, or synthesized to form star, brush, or grafted polymers. Diblock and triblock copolymers are currently the most extensively studied block copolymers. The blocked arrangement of monomers can be beneficial to many applications and can offer interesting features. A noteworthy property that block copolymers can exhibit is amphiphilicity. Monomers of distinct polarities must be chosen to synthesize a block copolymer of amphiphilic nature. Representative monomers for hydrophobic blocks can be styrene, butadiene, butylene oxide, and propylene oxide or polylactic acid. For the hydrophilic building block, the chosen monomer should be of a high polarity, such as acrylamide, acrylic acid, methacrylic acid and hydroxyethyl methacrylate.[2,3] Amphiphilicity is property of great interest for the pharmaceutical industry, the food industry, the cosmetics industry, and material science.[4] Furthermore, amphiphilicity can facilitate the formation of self-assembled structures, such as polymeric micelles. Previous studies have demonstrated that micelles of polymeric nature are more stable than micelles formed from conventionally used small molecule surfactants. This allows them to solubilize hydrophobic substrates.[5] These features make amphiphilic block copolymers interesting candidates for the use as so-called ”macrosurfactants”, which can stabilize emulsions effectively, allowing the synthesis of polymerized high- and medium-internal phase emulsions.[6] Moreover, amphiphilic block copolymers may be used as "polymer drag-reducing agents" (DRAs). These are employed to decrease frictional drag in pipe flow. One notable area of application is hydraulic fracking, in which substantial quantities of fluids are transported through pipes at a high velocity. The energy required for the transport of these fluids can be reduced using DRAs.[7] However, a current

limitation of DRAs is that they often have adverse environmental effects and are not easily removable or recoverable from solutions.[8]

1.2 Project Aim

The objective of this study is to synthesize a copolymer, poly(acrylamide-co-styrene), for application as a macrosurfactant. The polymer will be synthesized via micellar polymerization, with the objective of using the polymer in its as-synthesized state, whereby a certain amount of surfactant from the synthesis remains associated with the polymer. The synthesized poly(acrylamide-co-styrene) will be used for the synthesis of MBAm/HEMA-based polyH/MIPEs. The aim is to reduce the quantity of emulsifier necessary for stabilization, thereby lowering costs and saving materials. The microstructure, porosity, and density of the resulting H/MIPEs will be investigated. The swelling capacity and mechanical properties will be tested, as well as self-removing properties and foaming characteristics of poly(acrylamide-co-styrene). Furthermore, poly(acrylamide-co-styrene) will be tested in the ViEDRA (Vienna Experiment for Drag Reducing Agents), with the aim of removing the polymer from the solution and extracting it as foam, supported by gel permeation chromatography measurements. The extracted foam will be dried, and its microstructure is going to be analyzed. With a foam analyzer, the structure and stability of the liquid foam will be investigated.

1.3 Theoretical Background

1.3.1 Definition of a Macrosurfactant

Amphiphilic polymers fulfil all the necessary criteria to act as a surfactant. According to IUPAC, a surface-active agent (short: surfactant) is “a substance which lowers the surface tension of the medium in which it is dissolved, and/or the interfacial tension with other phases, and, accordingly, is positively adsorbed at the liquid/vapor and/or at other interfaces“.[9] Figure 1 illustrates this phenomenon. A surfactant influences the interfacial tension at liquid/gas (L/G) and liquid/liquid (L/L) interfaces by adsorbing to the interface. The molecular interactions between the two phases are reduced. At the L/G interface, for example water/air, the hydrophilic parts orient themselves towards the liquid phase.[10]

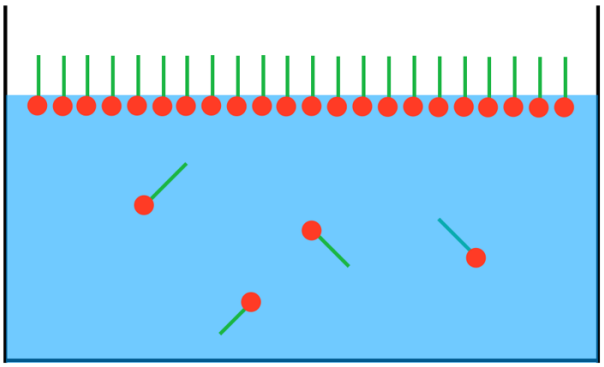

Figure 1 - The arrangement of the surfactant molecules at an air-water interface

Compared to commercially available surfactants such as CTAB, Tween (polysorbates) and Span (sorbitan esters), polymeric surfactants exhibit a greater structural flexibility. The arrangement and distribution of building blocks have a significant influence on the behavior of the polymer in solution and represent an important parameter for regulating the polymers properties. Surfactants of polymeric nature can be classified into two general categories, macrosurfactants and “polysoaps”, depending on the distribution of hydrophilic and hydrophobic moieties over the polymer backbone. Polymers that exhibit a distinct separation of the two moieties are designated macrosurfactants. Conversely, polymers that contain inherently amphiphilic building blocks are classified as "polysoap”.[11] A broad range of monomers and sophisticated synthesis techniques offer considerable scope for the synthesis of polymeric surfactants. Figure 2 provides examples of macrosurfactants from the literature.

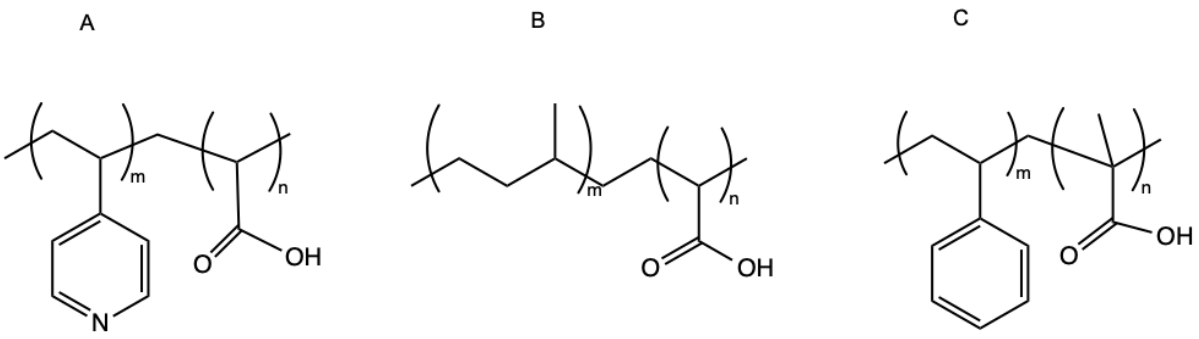

Figure 2 – A) P4VP-b-PAA[12], B) PhIP-b-PAA[13], C) PS-b-PMAA[14]

Poloxamers, also known as Pluronics, serve as another example of an amphiphilic polymer. Poloxamers are nonionic triblock copolymers, comprising a hydrophobic poly(propylene oxide) block that is flanked by two hydrophilic poly(ethylene oxide) blocks. This results in an amphiphilic nature, accompanied by the capacity to form self-assembled structures. While macrosurfactants form micelles based on side chains or segmented structures, Pluronics, such as poloxamers, utilize the triblock structure, resulting in distinct micelle formation mechanisms.[15]

1.3.1 Properties of Macrosurfactants

Macrosurfactants, such as polymeric surfactants, have a more complex structure compared to their low-molecular weight counterparts. Their properties in aqueous solution can be adjusted by the distribution of the hydrophobic and hydrophilic moieties along the polymer backbone. Surfactants can form self-assembled structures, greatly depending on the concentration and solvent system they are employed in.[16] Due to their structural flexibility, polymeric surfactants can assemble into more complex structures as the long-chain structure allows the polymer to adapt various conformations. This enables the formation of micelles with different shapes, sizes, and arrangements.[17] Their ability to form micellar structures, their impact on surfaces, and their emulsifying properties will be discussed in the following chapters.

1.3.1.1 Formation of Micellar Structures and the critical micelle concentration

The critical micelle concentration (CMC) is the concentration at which micelle formation occurs. The CMC is not solely dependent on the surfactant concentration; when polymers are used as surfactants, the CMC is also dependent on the polymer architecture, including its hydrophobic and hydrophilic moieties. The results of computational modeling demonstrated that the CMC decreases with the length of the hydrophobic block, while the influence of the hydrophilic block appears to be negligible.[18] Lee et al.[19] reached comparable conclusions. Copolymers of PNiPAAm (poly(N-isopropylacrylamide)), which functioned as the hydrophilic comonomer, were subjected to testing. As a hydrophobic monomer, a variety of caprolactone (CL) derivatives were employed. It was observed that an increase in the length of the CL blocks resulted in a notable reduction of the CMC.[19] In contrast to this stand, what was experimentally determined by Mok et al.[18] They state that CMC ≈ exp(-cN) for low N with c as a Flory-Huggins dependent parameter and N as the length of the hydrophobic block. Higher values of N lead to a lower dependence of CMC on the

Flory-Huggins parameter. The CMC then follows $\exp(-cN^{1/3})$.[18] This indicates that the impact of the hydrophobic block on the CMC is less pronounced than previously anticipated. Comparing the results of these two studies, it is noticeable that their results are inconsistent, indicating that the most important parameter in achieving CMC remains polymer concentration.

Polymeric surfactants have made it possible to discover a variation of geometries of micelles like multicompartment micelles, inverse micelles, and special spherical micelles.[20] Polymeric vesicles have been of great interest, as they can successfully be employed as carriers for drugs. The versatility of available monomers enables a great spectrum of variety in the architecture of macrosurfactants, which is an advantage compared to small molecule surfactants. The nature of the resulting micelle is greatly influenced by the design of the block copolymer. Garnier et al.[20] state that co-polymers comprising the same hydrophobic monomer (butyl acrylate) but having various hydrophilic blocks (acrylic derivatives) formed micelles depending on the block length of the hydrophilic monomer. No significant influence of the molecular architecture of the hydrophilic monomer on micelle formation was reported.[20] However, the findings of Zhang et al.[21], who were working with identical hydrophobic blocks but different hydrophilic blocks, arrived at the opposite conclusion. Their findings indicated that the formation of micellar structures was primarily influenced by the molecular structure of the hydrophilic monomer.[21] For this reason, the precise influence of block length and molecular architecture of the employed monomer remains unclear and appears to be dependent on more than those two factors.

1.3.1.2 Effect of Macrosurfactants on Surface- and Interfacial Tension

Macrosurfactants in aqueous solution cause a decrease in surface- and interfacial tension. A schematic representation can be found in Figure 3. This observation can be made for all surfactants, as the decrease in surface tension is a result of the amphiphilic nature of the employed surfactant molecule. The surface tension continues to decrease until the CMC is reached. The surface/interface is then saturated, and a plateau is reached, where further addition of surfactant does not influence the surface tension/interfacial tension and micelles form.[22]

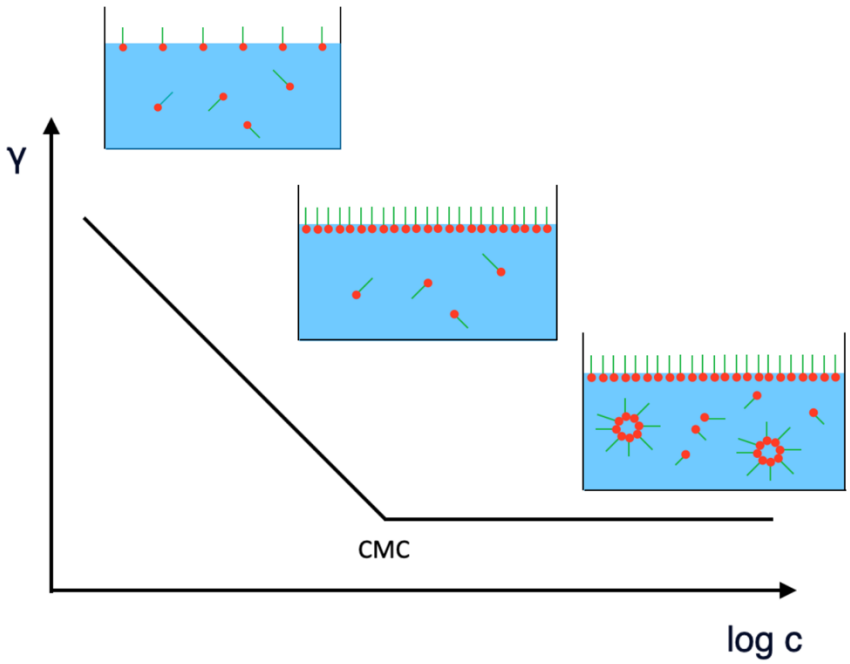

Figure 3 – Surface tension or interfacial tension (γ) decrease with increasing surfactant concentration. Once the critical micelle concentration (CMC) is exceeded, a plateau is reached and no further decrease of γ occurs.

The hydrophobic part or block of the surfactant molecule will be directed towards air or non-polar immiscible liquid, while the polar part will point towards the aqueous phase. The disruption of the air-water or water-nonpolar liquid interface decreases the corresponding surface/interface tension.

1.3.1.3 Emulsifying Properties

According to IUPAC, an emulsion is defined as: "A fluid colloidal system in which liquid droplets and/or liquid crystals are dispersed in a liquid".[23] Emulsions can be divided into two main categories: oil-in-water (o/w) and water-in-oil (w/o) emulsions. In an o/w emulsion, the oil phase is dispersed in a continuous aqueous phase, whereas in a w/o emulsion, the aqueous phase is dispersed in a continuous oil phase.[24] Emulsions can be further classified according to the relative volume fractions of the two phases. HIPEs are defined as emulsions containing at least 70% internal phase, with the remainder being the external phase. Emulsions with less than 70% internal phase are classified as MIPE. Emulsions with less than 30% internal phase are designated LIPE.[25]

1.3.1.4 Emulsion Templating: From Emulsions to Porous Polymers

Emulsion templating is a frequently utilized technique for the fabrication of porous polymers. In this method, the continuous phase, which contains the dispersed internal phase, is polymerized. After the removal of the internal phase, a micro- to macroporous monolith can be obtained. The phase volume ratio offers control over the porosity of the resulting polymer monolith, while the pore size is controlled by the energy input, thereby influencing the monoliths' mechanical properties. The aforementioned facts make polyH/MIPEs an interesting option, for example in tissue engineering of bones and a multitude of separation processes.[26,27,28]

1.3.2 Amphiphilic Polymers for Drag Reduction Applications

A variety of chemical substances can be employed as drag-reduction agents (DRAs). Amongst these, polymers have demonstrated great efficacy.[29] Amphiphilic polymers have been studied in the past years because they have a potential to reduce drag in turbulent flow.[30] This is because of their ability to form aggregates of high molecular weight, dependent on the concentration range used. However, a current challenge in research is that many polymers degrade over time in flowing systems. The degradation process may be delayed if polymers are used, which are able to form aggregates, with “sacrificial bonds”.[31]

1.3.2.1 Mechanisms of Polymer-Based Drag Reduction

Several theories have been proposed to describe the mechanism of drag reduction with polymers. One model worth mentioning is the viscous model, which was proposed by Lumley et al. [32] The hypothesis suggests that the stretching of polymer coils in a turbulent flow can result in energy absorption. This leads to a disruption of the vortex cascade, thereby reducing the turbulences.[32]

1.3.2.2 Hydraulic Fracturing

Hydraulic fracturing, commonly called "fracking," was initially developed over six decades ago by Halliburton to enhance oil and gas production. Since its earliest applications, hydraulic fracturing has proven to be an effective technique with a global prevalence in oil and gas production. During the process, a fluid known as a "fracking fluid" is injected into the well at high pressure, creating fissures in the reservoir, enhancing the extraction of oil and gas. Fluids of various types are used for fracking. These include for example commercially available surfactants and emulsions, and

aqueous polymer solutions. [33] Polyacrylamide (PAM) is a frequently used polymer in hydraulic fractioning. [34] Like most polymers of high molecular weight, acrylamide-based polymers degrade because of exposure to high shear or other mechanical stress. Mechanical degradation is a non-reversible process that results in the fragmentation of the polymer chain into shorter fragments.[35,36] This highlights the urgent need for a polymer with a resistance to degradation in shear flow, that can be recovered from solutions and reused with similar efficiency.

2 Experimental Methods

2.1 Materials

Acrylamide and methanol used for the synthesis of P(AAm-co-St) were purchased from Sigma Aldrich. Acetone, used for the purification of acrylamide (via recrystallization), was purchased from Sigma Aldrich. For polymer synthesis, styrene, $K_2S_2O_8$ (potassium persulfate) and CTAB (cetyltrimethylammonium bromide) purchased from Sigma Aldrich, were used. Toluene, cyclohexane, 2-hydroxyethyl methacrylate (HEMA), N,N-methylenebisacrylamide (MBAm), N,N,N',N'-tetramethyl ethylenediamine (TEMED) and ammonium persulfate (APS), also purchased from Sigma Aldrich were used to synthesize HEMA/MBAm based polyH/MIPEs. Triton X-405 (polyethylenglycol tert-octylphenylether, 70% in H_2O), purchased from Sigma Aldrich, and polyvinyl alcohol (PVA), M_w = 15 kg/mol, purchased from Thermo Fisher Scientific were used to synthesize comparative samples following a published recipe.[42] During the polymer synthesis, nitrogen (Messer) was used to create an inert atmosphere in the Schlenk line. The dialysis to purify the synthesized copolymer was performed with dialysis bags from Thermo Fisher Scientific (molecular weight cut-off = 8000 Da). Deionized water (DI) was used, derived from a Water Purifier by Elga. For the GPC measurements, Dextran (M_w= 69·10^3 g/mol) and polyethylene oxide (M_w = 24·103 g/mol) standards were used, purchased from Malvern. Dishwasher salt (Tandil) was bought from Hofer.

2.2 Synthesis of Poly(acrylamide-co-styrene)

For the synthesis of poly(acrylamide-co-styrene) (P(AAm-co-St) 50 mL of DI was filled into a 250 mL round-bottom flask. 3.5 g CTAB (9.60 mmol) was added and dissolved under constant stirring at room temperature. The mixture was stirred at a low speed to avoid foaming. In the following step, styrene was added. Depending on the desired hydrophobic moieties in the final polymer, the following amounts of styrene were added as given in Table 1:

Table 1 - Mass of styrene added to the reaction to achieve the corresponding mol.% of hydrophobic moiety

mol.% Styrene	**Styrene [g]**	**Styrene [mmol]**
2	0.0745	0.715
4	0.149	1.431
7	0.260	2.496
11	0.410	3.937

Once styrene had been added to the flask, the mixture was stirred overnight at room temperature. The following day, 2.5 g of acrylamide (35.17 mmol) was added to the mixture and stirred until the acrylamide was fully dissolved. The flask was subsequently closed and connected to a Schlenk line, and the reaction mixture was subjected to freeze-pump cycles. Following the completion of three cycles, the reaction mixture was heated to 80°C. Once the temperature was stable, 2 mL of aqueous $K_2S_2O_8$ solution (88.25 mg, 0.33 mmol) was added dropwise under an inert atmosphere. The flasks were covered in aluminum foil to protect the reaction mixture from light. This is necessary as UV or visible light can cause the formation of unwanted radicals. These radicals can interact with the polymer radicals and terminate the growing chains prematurely, leading to a poor control over the molecular weight.[37] After 24 h, the reaction mixture was poured into methanol under constant stirring to precipitate the polymer. The polymer was subsequently purified using two distinct methods. These two methods are described in detail in 2.2.2 and 2.2.3.

2.2.1 Structural Analysis via ^{1}H-NMR

An aliquot of the dry, synthesized polymer was dissolved in D_2O by shaking overnight at 300 rpm. The NMR spectra were recorded with a 600 MHz NMR (BioSpin by Bruker). NMR spectra were then evaluated using TopSpin 4.0.9 software. In Table 2, the integrals of the methylene and phenyl groups used in equation 1 are clarified.

Table 2 – Explanation of integrals used in Equation 1 to calculate St (mol%).

Integral	**Source of signal**
$I_{7.3ppm}$	Integral of triplet resulting $-C_6H_5$
$I_{1.5-1.8ppm}$	Integral of protons from $-CH_2$ (polymer backbone)

2.2.2 Purification Route for the as-synthesized Polymer

In this work, the polymer referred to as as-synthesized polymer was collected from methanol after precipitation and transferred to another beaker. The polymer was then dissolved in a minimum of DI on a shaker (PSU-10i, Biosan) at 300 rpm overnight. On the following day, the aqueous polymer solution was transferred to Falcon tubes. The polymer was then dried with a benchtop freeze dryer (LyoQuest by Telstar).

2.2.3 Purification Route for the Purified Polymer

The polymer, which in this work is referred to as “purified” was purified as the as-synthesized polymer in the initial steps. Then, instead of immediate freeze drying, the aqueous polymer solution was transferred into dialysis tubes. The tubes were kept in DI for 10 days. The DI was exchanged three times per day to ensure sufficient purification. After purification, the polymer was recovered via lyophilization. The purity of the polymer was determined by indirectly measuring the amount of residual surfactant associated to the polymer with elemental analysis as detailed in Appendix C.

2.3 Measurement of Interfacial Tension Between Toluene and Water

Aqueous solutions with concentrations ranging from 0.001 to 1 wt.% of as-synthesized P(AAm-co-4St) (P(AAm-co-St) with 4 mol% of styrene), purified P(AAm-co-4St), and purified P(AAm-co-4St) with CTAB added were used to investigate the decrease of interfacial tension between toluene and water. All solutions were prepared using DI water. The measurements were conducted using a tensiometer (K100 by Krüss) employing the Wilhelmy plate method.

2.4 Preparation of H/MIPEs

Aqueous solutions of the PAM homopolymer and P(AAm-co-St) were prepared by weighing the polymer to beakers and dissolving it in DI on a shaker at 300 rpm overnight, producing concentrations ranging from 0.001 to 1 wt.%. The polymer solution (either as-synthesized P(AAm-co-4St) (P(AAm-co-St) with 4 mol.% of styrene), purified P(AAm-co-4St) or purified P(AAm-co-4St) with additional CTAB)) was then transferred to a Falcon tube. HIPEs comprising 75% toluene and 25% aqueous polymer solution were produced by vortexing the mixture for 10 min, while adding toluene dropwise with a glass pipette.

2.5 Synthesis of PolyH/MIPEs

For the synthesis of the polyH/MIPEs, the aqueous polymer solution was transferred into a 50 mL Falcon tube. Ammonium peroxodisulfate (APS) was weighed and added to the solution. The mixture was vortexed until the APS had been fully dissolved. In case of the purified polymer with additional CTAB, the CTAB was added when making the stock solution of the polymer. HEMA and MBAm were added to the solution and again, vortexed until all components had fully dissolved. The internal phase (cyclohexane) was added dropwise with a rate of 1 drop per min. Once the addition of cyclohexane was finished and a stable emulsion was obtained, TEMED was added. Immediately after the addition of TEMED, the tube was closed and vortexed until a rise in temperature of the mixture was noticeable. The tube was then left to polymerize for 1 h at room temperature. The tubes were then opened and placed into to a convection oven at 60°C overnight. This step served to remove the cyclohexane from the obtained monolith. After pre-drying, the residual cyclohexane was then removed by drying the monoliths in a vacuum oven at

room temperature for two days. The recipes for the polyH/MIPEs that were produced in the course of this work are given in Table 3:

Table 3 – Composition of all polyHIPEs and polyMIPEs that were made in the course of this work. P1-P3 are polyHIPEs, P4-P6 are polyMIPEs. These emulsions were stabilized by adding purified P(AAm-co-4St) with additional CTAB. P7-P9 and P7'-P9' are polyHIPEs, stabilized by as-synthesized P(AAm-co-4St). P10-P12 are polyMIPEs, also stabilized by as-synthesized P(AAm-co-4St), without any additional CTAB.

	Aqueous phase								Oil Phase
	H_2O [wt.%]	**As-synthesised P(AAm-co-4St) [wt.%]**	**Purified P(AAm-co-4St) [wt.%]**	**CTAB [wt.%]**	**MBAm [wt.%]**	**HEMA [wt.%]**	**APS [wt.%]**	**TEMED [wt.%]**	**Cyclohexane [wt.%]**
P1	20.54	-	0.15	0.10	1.22	7.53	0.24	0.12	70.1
P2	20.39	-	0.15	0.10	1.72	7.03	0.34	0.17	70.1
P3	20.33	-	0.15	0.10	1.93	6.82	0.38	0.19	70.1
P4	28.72	-	0.10	0.10	1.63	10.37	0.32	0.16	58.6
P5	28.51	-	0.10	0.10	2.34	9.66	0.46	0.23	58.6
P6	28.42	-	0.10	0.10	2.64	9.36	0.52	0.26	58.6
P7	20.64	0.15	-	-	1.22	7.53	0.24	0.12	70.1
P8	20.49	0.15	-	-	1.72	7.03	0.34	0.17	70.1
P9	20.43	0.15	-	-	1.93	6.82	0.38	0.19	70.1
P'7	20.69	0.10	-	-	1.22	7.53	0.24	0.12	70.1
P'8	20.54	0.10	-	-	1.72	7.03	0.34	0.17	70.1
P'9	20.48	0.10	-	-	1.93	6.82	0.38	0.19	70.1
P10	28.82	0.10	-	-	1.63	10.37	0.32	0.16	58.6
P11	28.61	0.10	-	-	2.34	9.66	0.46	0.23	58.6
P12	28.52	0.10	-	-	2.64	9.36	0.52	0.26	58.6

2.6 Characterization of PolyH/MIPEs

2.6.1. Characterization of Porosity and Density

Initially, the density was determined by pycnometry. The envelope density ρ_f was determined using a sand displacement pycnometer (Geopyc 1360, Micrometrics). The skeletal density was determined using helium pycnometry (Accupyc 1330 by Micrometrics). For each sample, a total of nine measurements were conducted. Subsequently, a mean value was calculated. The porosity was calculated, following equation 1:

$$P(\%) = \left(1 - \frac{\rho_f}{\rho_s}\right) \times 100 \qquad (1)$$

2.6.2 Analysis of the Microstructure

The microstructure of the liquid emulsions of high- and medium-internal-phase, produced with toluene, was examined using a light microscope (DM2700 M by Leica). The microstructure of the solid PolyH/MIPEs was characterized via scanning electron microscopy (SEM) (JCM-6000 by JEOL) with acceleration voltage of 15 kV and distance to lens varying from 20-50 µm. The PolyH/MIPEs are not electrically conductive. A subsample of each specimen was mounted on a sample holder with a double-sided adhesive carbon sticker. Subsequently, the sample was coated with a thin layer of gold to ensure a conductive surface, necessary for the SEM. To determine the pore and pore throat diameter, ImageJ software was used to quantify the number of pores.

2.6.3 Water Swelling Capacity

The polyH/MIPEs were characterized regarding their water swelling capacity (Q). The polyH/MIPEs were cut into uniform pieces of 23 mm and height of 10 mm with a diamond knife. The samples were immersed in deionized water and left to swell for up to 18 hours. Three pieces were tested per monolith and a mean value was calculated. The water uptake was determined during the swelling process by measuring the sample dimensions and weighing at fixed time intervals. The dimensions were measured until no significant change in mass was observed. The swelling capacity Q was calculated as the change of mass (m_s = mass of sample after swelling, m_d = mass of dry sample), given in equation 2:

$$Q = \frac{m_s - m_d}{m_d} \quad (2)$$

These experiments were carried out for polyH/MIPEs P7-9, P7'-9' and P10-12 and for polyH/MIPEs, which were previously compressed to see if mechanical stress caused a change in the water swelling capacity.

2.6.4 Compression Tests

Compression tests were conducted on uniform pieces of the monoliths, which were cut with a diamond knife (23 mm diameter and 10 mm in height). All tests were carried out using the Instron 5969 (by Instron), a dual column universal testing frame. The stress-strain curves were recorded with a 1 kN load cell, and the samples were compressed to 70% of their height at a rate of 1 mm/min. PolyH/MIPEs (P8, P8' and P11) previously swollen in DI, were subjected to testing. The samples were exposed to loading and unloading cycles (cyclic compression), at a rate of 1 mm/min and with a strain of 50%. The recorded stress-strain curves were analyzed to determine the elastic moduli E_c and crush strength σ_c values.

2.7 Methods of Liquid Foam Preparation

2.7.1 Foaming Properties of P(AAm-co-St) and the Acrylamide Homopolymer

The ability of P(AAm-co-St) with different styrene contents to stabilize foam was tested. The polyacrylamide homopolymer (M_w = 10^6 g/mol) was taken as a control sample. The polymers were dissolved in a 0.1 M NaCl solution, as previously described in 2.4. Solutions were prepared in concentrations ranging from 100 to 3000 ppm. To determine which polymer was stabilizing the foam the most effectively, 10 mL of each solution was transferred to a glass vial and shaken by hand for 10 min.

2.7.2 Removal of P(AAm-co-St) from Aqueous Aolutions

ViEDRA (Vienna Experiment for Drag Reducing Agents) was used to test P(AAm-co-St) self-removal from aqueous solution. The facility's configuration is described in detail in the referenced source.[38] The ViEDRA tank was filled with a solution of 0.1 M NaCl, to a volume of

220 L. P(AAm-co-4St) was added to the solution and was subsequently stirred for 24 h. On the following day, the solution was forced through a pipe test section (7.2 m long) using compressed air. The solution was transported 20 m with each pumping cycle. This process was repeated 150 times, resulting in the polymer foaming the solution. The foam was collected in the mixing tank at regular intervals, approximately every five cycles.

2.8 Characterization of the Dry and Liquid Foam Structure

2.8.1 Characterization of Liquid Foam

The foam was extracted from the solution in the ViEDRA tank and subsequently characterized using a foam analyzer (DFA100, Krüss). The time-dependent foam volume (V_F) and the ratio of foam to liquid volume (V_T) were determined, along with the mean bubble area and the statistical distribution of bubbles.

2.8.2 Characterization of Dry Foam Microstructure

To analyze the microstructure, the collected foam was dried following two distinct methods: by drying at room temperature for approximately 5h or by freeze-drying overnight. The dried foam was analyzed via scanning electron microscopy (SEM). The preparation of samples and the subsequent measurements were carried out following the methodology previously outlined in 2.6.2.

2.9 Analysis of the Molecular Weight via Gel Permeation Chromatography

Gel permeation chromatography (GPC, Viscotec TDA 302, Malvern) equipped with OmniSEC 5.02 software for evaluation was used to assess the molecular weight and polydispersity of freshly synthesized P(AAm-co-St) and P(AAm-co-St), which was recovered and collected from the ViEDRA tank. The columns which were used for the separation are shown in Table 4:

Table 4 - Chromatography columns and their exclusion limits (kg/mol), with A-Guard separating based on hydrodynamic volume V_h.

Column	Exclusion limit [kg/mol]
A-Guard, Viscotek, Malvern	/ (separation based on V_h)
A4000	1000
A6000M	20000

As an eluent, a solution of sodium nitrate ($NaNO_3$) with a concentration of 0.1 M and sodium azide (NaN_3) with a concentration of 0.02 wt.% in DI was used. All measurements were carried out at 30°C and a flow rate of rate 0.7 mL/min. Dextran (M_w = 68991 g/mol) and polyethyleneoxide (PEO, M_w = 23651 g/mol), both purchased from Malvern, were used as calibration standard.

3 Results and Discussion

3.1 ^{1}H-NMR Analysis of P(AAm-co-St)

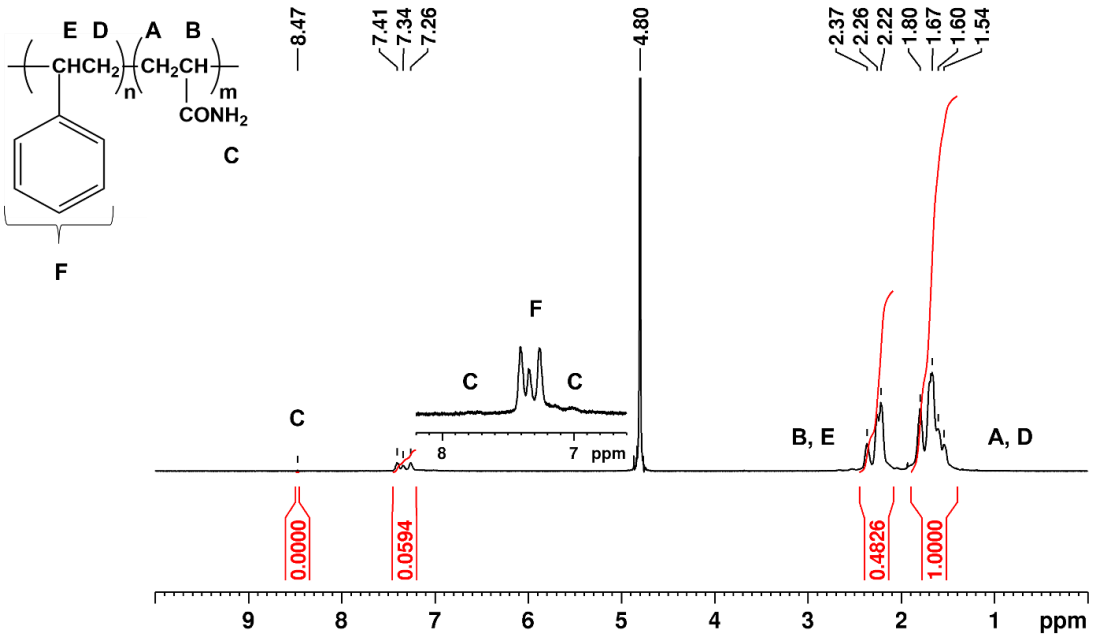

Figure 4 - ^{1}H-NMR spectrum of P(AAm-co-4St), recorded in D2O.

Figure 4 illustrates the ^{1}H-NMR spectra and the structure of P(AAm-co-4St). The amount of styrene in the synthesized polymer was calculated using Equation 3.

$$St\ (mol\%) = \frac{2I_{7.3\ ppm}}{3I_{1.5-1.8\ ppm} + 2I_{7.3\ ppm}} \times 100 \qquad (3)$$

All peaks are labeled regarding their proton environments. It can be observed that the aromatic protons, labeled F, are situated between 7 and 8 ppm, which is characteristic of aromatic hydrogens. The aromatic ring is a conjugated system. The delocalization of electrons affects the electron density, deshielding the protons and resulting in a significant downfield shift. The peaks labeled A, B, D, and E correspond to the aliphatic protons. These can be found in a range of 1-3 ppm, indicating the presence of methine groups (-CH) and methylene groups (-CH_2), as shown in Figure 4. Peaks labeled with C are the result of protons that belong to the amide group (-$CONH_2$). The amide protons resonate at a higher ppm, due to the electron-withdrawing nature of the carbonyl group, which is deshielding the protons. Following equation 2, the styrene moieties was calculated.

3.2 Emulsifying Properties of P(AAm-co-St)

The emulsifying properties of P(AAm-co-St) were tested through emulsion templating. Initially, the homopolymer (polyacrylamide), P(AAm-co-2St) and P(AAm-co-4St), were evaluated to assess whether there was a noticeable difference in their emulsifying properties. In total, six HIPEs were tested, with two samples prepared for each polymer at concentrations of 0.01 and 0.1 wt.% (0.1 wt% ≈ $8.1 \cdot 10^{-7}$ mol/L, 1 wt% ≈ $8.1 \cdot 10^{-6}$ mol/L based on 15 g total weight of emulsion and M_w(P(AAm-co-4St) ≈ 370000 g/mol). Figure 5 presents the resulting emulsions.

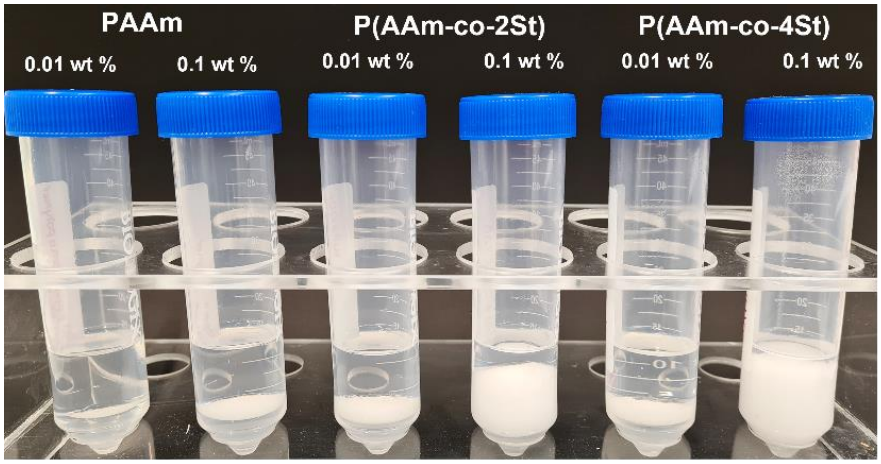

Figure 5 - HIPEs comprising 75% toluene and 25% water, stabilized with 0.01 wt.% or 0.1 wt.% of homopolymer (polyacrylamide), (P(AAm-co-2St) or P(AAm-co-4St) in the aqueous phase.

It can be observed that the homopolymer lacks emulsifying properties. At a dilution of 0.01 wt.%, no emulsion forms. At a concentration of 0.1 wt.%, a minimal quantity of the aqueous phase was emulsified. Better results can be observed in the case of (P(AAm-co-2St) and P(AAm-co-4St). Already a concentration of 0.01 wt.%, the emulsifying properties of P(AAm-co-2St) appear comparable to that of the homopolymer at a concentration of 0.1 wt.%. This indicates that (P(AAm-co-2St) shows comparable emulsifying properties at a concentration ten times lower than the homopolymer. At a concentration of 0.1 wt.% both phases were fully emulsified. The observed effect is even more pronounced for P(AAm-co-4St). At a concentration of 0.1 wt%, most of the oil and water phases were emulsified, with minimal excess of either phase. For this reason, P(AAm-co-4St) was selected as emulsifier for all following experiments, such as the synthesis of polyH/MIPEs and production of foam.

As demonstrated in Figure 6, the addition of CTAB to the aqueous phase led to enhanced emulsification. It was observed that a stable HIPE was produced at a concentration of 0.1 wt.% P(AAm-co-4St) + 0.01 wt.% CTAB, whereby the oil and water phases were fully emulsified. No significant change was observed after increasing the concentration of CTAB to 0.02 or 0.05 wt.%. For 0.1 wt.% of (P(AAm-co-4St) + 0.1 wt.% CTAB, an extremely dense, almost jelly-like HIPE was obtained.

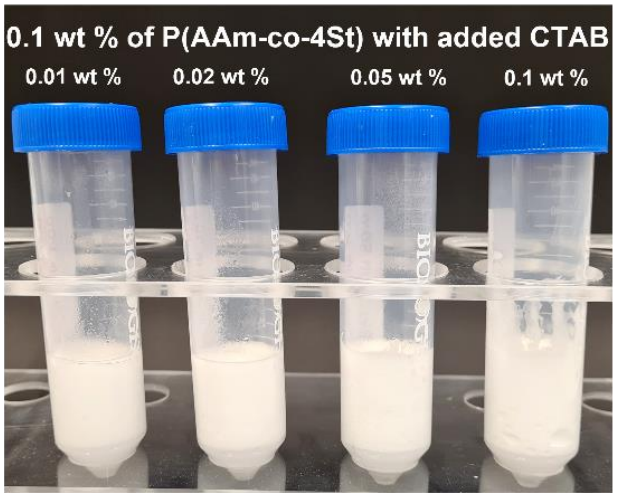

Figure 6 - HIPEs comprising 75% toluene and 25% water, stabilized with 0.01 wt.%-0.1 wt.% of P(AAm-co-4St) and 0.1 wt.% CTAB in the aqueous phase.

As a control sample HIPEs were produced by using solely CTAB to stabilize the emulsions. The resulting HIPEs are shown in Figure 7. It is very noticeable that water is still resting on the bottom of the tubes. The resulting emulsions had a low viscosity. Using solely CTAB as a surfactant was less efficient than combining CTAB and P(AAm-co-4St).

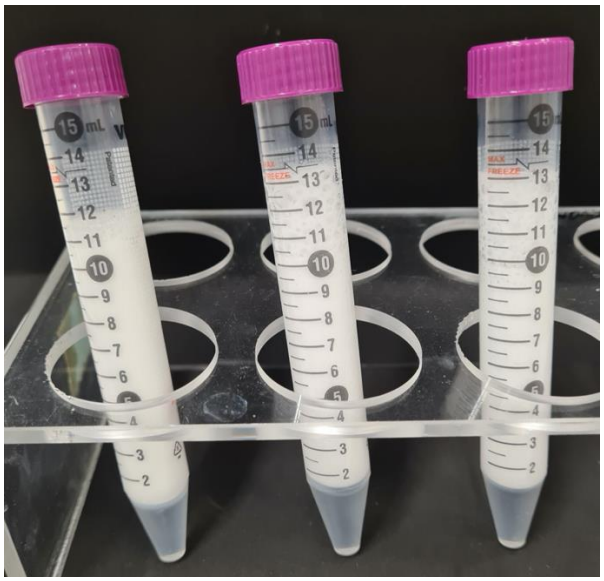

Figure 7 – Replicated of toluene/water 75/25 vol.%, stabilized by 0.1 wt.% CTAB.

3.3 Interfacial Tension of Toluene/Water HIPEs, stabilized by P(AAm-co-4St)

Figures 8 and 9 present the interfacial tension of the toluene/water interface as a function of the polymer concentration. For purified P(Aam-co-4St), a linear trend can be observed. As the polymer concentration increased, the interfacial tension decreased, confirming that the polymer functions as a macrosurfactant.[23]

As-synthesized P(Aam-co-4St), shows a behavior that is distinct from that observed with the purified P(Aam-co-4St), as the as-synthesized P(AAm-co-4St) is still associated with residual CTAB from the synthesis. It is observed that the as-synthesized P(AAm-co-4St) shows a more pronounced reduction of the interfacial tension compared to the purified P(AAm-co-4St). The stronger reduction of the interfacial tension is evident even at a concentration of 0.001 wt.% as-synthesized P(AAm-co-4St). At concentrations of 0.1 wt.%, as-synthesized P(AAm-co-4St) approaches interfacial tensions of 0 mN/m. This is a notable contrast to the behavior observed in purified P(AAm-co-4St), which reduced interfacial tension to approximately 22.5 mN/m at a concentration of 0.1 wt.%. At a concentration of 1 wt.%, the reduction in interfacial tension appears to reach a plateau, suggesting that saturation of the polymer on the interface may set in. In contrast to the purified P(AAm-co-4St), the as-synthesized P(AAm-co-4St) is precipitated only once in methanol following the synthesis. It is then dissolved in DI and lyophilized. P(AAm-co-4St) was synthesized by micellar polymerization, using CTAB as the surfactant of choice. CTAB has a long and hydrophobic tail (C16) as well as a quaternary ammonium head group. This structure makes it efficient at forming stable micelles. These micelles function as reactors within which the polymerization takes place.[39] Excluding any additional precipitation or dialysis stage leads to 0.01 wt.% residual CTAB remaining associated with the dried polymer. The observed reduction of interfacial tension is, therefore, a consequence of the interaction between CTAB and P(AAm-co-4St). The polymer-surfactant interaction facilitates the reduction of the interfacial tension. Commercially available CTAB, a small-molecule surfactant, demonstrated a more efficient reduction of the interfacial tension at low concentrations than the purified and as-synthesized P(AAm-co-4St). At concentrations of 0.1 and 1 wt.%,the unpurified P(AAm-co-4St) demonstrated a superior reduction of interfacial tension compared to solely CTAB.

Figure 9 illustrates the interfacial tension of purified P(AAm-co-4St) in the presence of additional CTAB as a function of the polymer concentration. The combination of purified P(AAm-co-4St) with a fixed amount of 0.1 wt.% CTAB proved to be more efficient than CTAB alone and also exhibited a higher reduction in interfacial tension than the as-synthesized P(AAm-co-4St). Once more, it seems that saturation occurs at a lower concentration, specifically at 0.01 wt.%. This may be a result of the higher CTAB concentration when added after synthesis compared to the amount of CTAB (0.01 wt.%) still associated with the as-synthesized P(AAm-co-4St).[40,41]

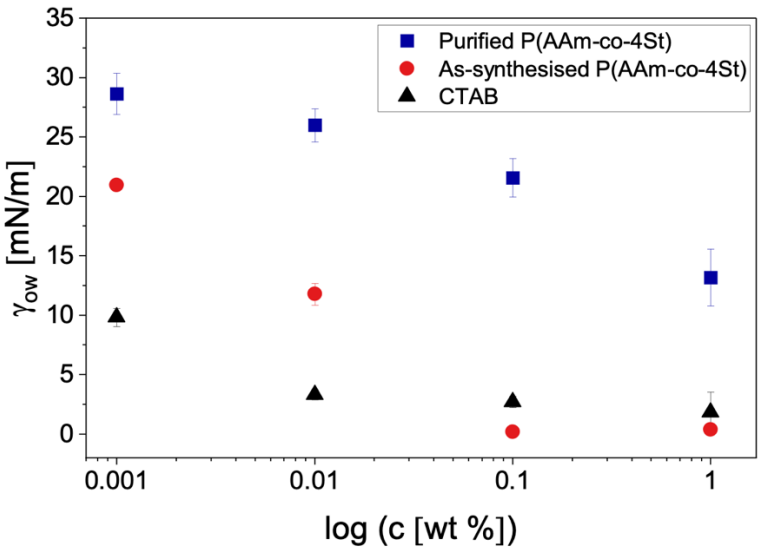

Figure 8 – Interfacial tension between toluene and the aqueous phase (containing either purified P(AAm-co-4St), as-synthesized P(AAm-co-4St), and solely CTAB) as a function of (macro) surfactant concentration.

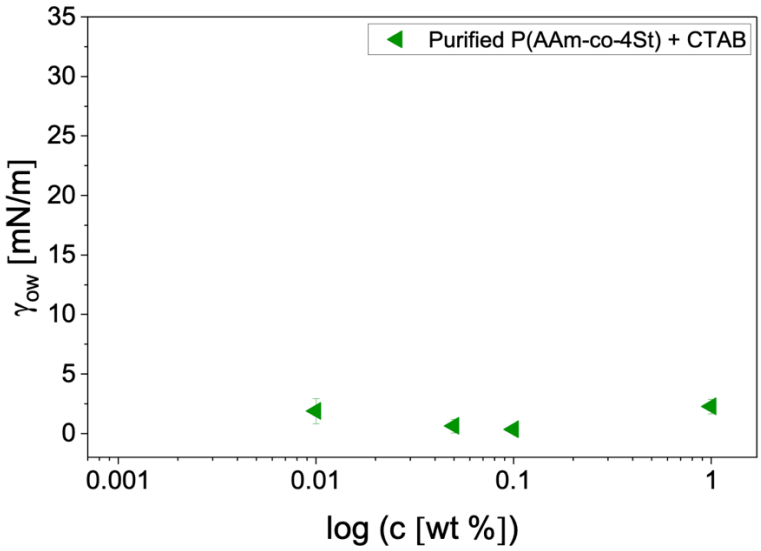

Figure 9 – Interfacial tension between toluene and the aqueous phase, containing purified P(AAm-co-4St) combined with CTAB as a function of the polymer concentration.

3.4 Analysis of the HIPE Microstructure with Light Microscopy

The microstructure of the HIPEs discussed in 3.1 was examined using light microscopy. Figure 10 illustrates the microstructure of a HIPE comprising 75% toluene and 25% water, stabilized by a) 0.01 wt.% and b) 0.1 wt.% polyacrylamide homopolymer ($M_w = 10^6$ g/mol). As illustrated in Figure 10a, stabilized by 0.01 wt.% polyacrylamide, it is evident that a lower degree of emulsification occurred, resulting in a sparse distribution of droplets. Figure 10b shows the microstructure of a HIPE comprising 75% toluene and 25% water, stabilized by 0.1 wt.% polyacrylamide homopolymer. In this case, an increased number of droplets was observed, forming clusters. Figures 11a and 11b present the HIPEs stabilized by 0.01 wt.% and 0.1 wt.% of P(AAm-co-2St), respectively. A distinct increase in the number and size of droplets was observed as the concentration of polyacrylamide homopolymer was increased from 0.01 to 0.1 wt.%. A comparison of the microscopy pictures of emulsions stabilized by polyacrylamide homopolymer and P(AAm-co-2St) shows, that P(AAm-co-2St) produces an emulsion of higher droplet density. Similar observations are made for emulsions stabilized by P(AAm-co-4St), which is depicted in Figure 12. It can be seen that at 0.01 wt.% P(AAm-co-4St) the emulsion already shows comparable characteristics to an emulsion stabilized by 0.1 wt.% P(AAm-co-2St). The defining characteristics of a HIPE are a high droplet density with a high packing efficiency.[43] This is not

observed for the homopolymer or P(AAm-co-2St). Nevertheless, characteristics of a HIPE are observable at 0.1 wt.% P(AAm-co-4St), as illustrated in Figure 12b.

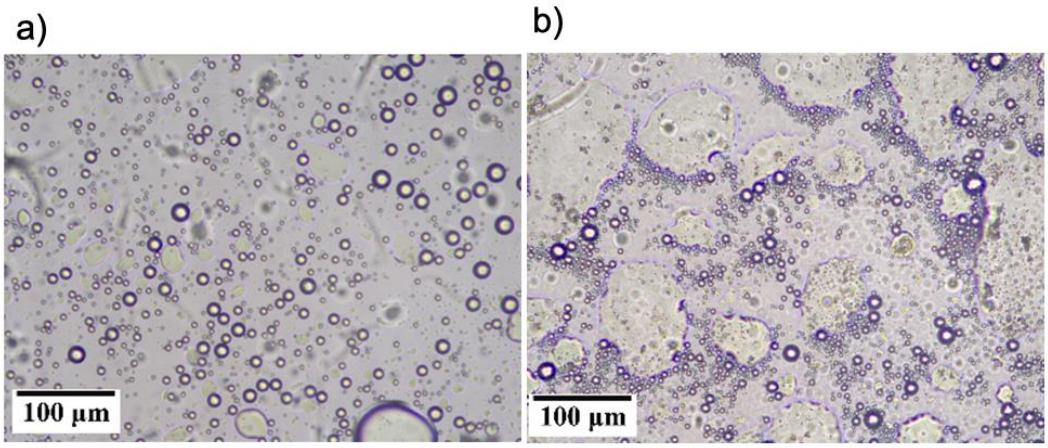

Figure 10 - HIPE comprising 75% toluene and 25% water, stabilized by a) 0.01 wt.% and b) 0.1 wt.% polyacrylamide

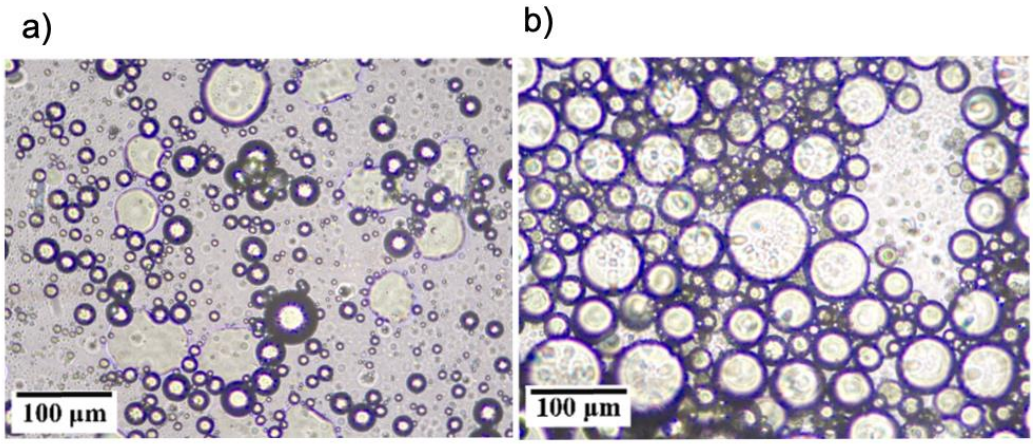

Figure 11 - HIPE comprising 75% toluene and 25% water, stabilized by a) 0.01 wt.% and b) 0.1 wt.% P(AAm-co-2St)

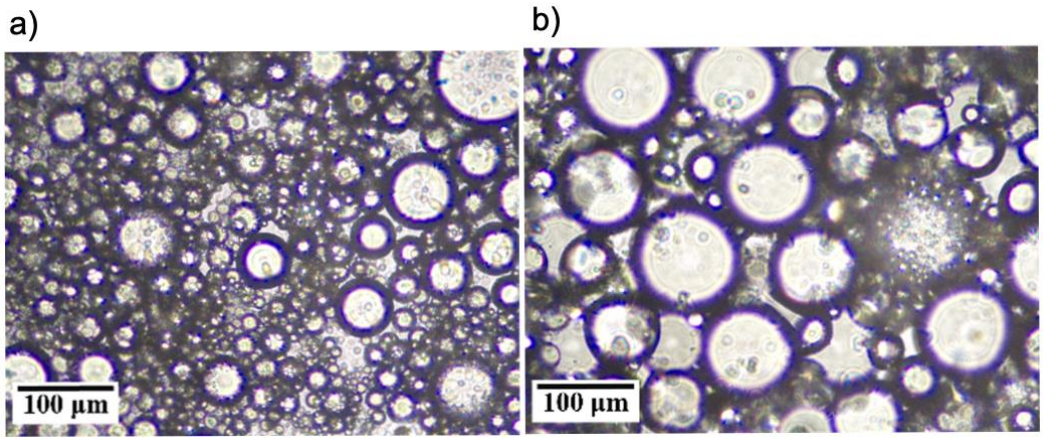

Figure 12 - HIPE comprising 75% toluene and 25% water, stabilized by a) 0.01 wt.% and b) 0.1 wt.% P(AAm-co-4St)

3.5 Synthesis of PolyH/MIPEs

The synthesis of the polyH/MIPEs was successfully carried out for all the recipes listed in Table 3. Uniform and even monoliths were obtained for each sample, as illustrated in Figure 13. The resulting monolith exhibited dimensional stability and minimal shrinkage.

Figure 13- polyHIPE stabilized by as-synthesised P(AAm- co-4St)

The control sample is shown in Figure 14. PolyHIPEs were reproduced according to the method described by Kulygin and Silverstein.[42] The resulting monolith exhibited significant deformation, an uneven surface, and lacked smoothness. Shrinkage was observed after drying.

Figure 14 – polyHIPE stabilized by 0.73 wt % PVA and 6.38 wt % Triton X-405, as described by Kulygin and Silverstein[42]

3.6 Analysis of the polyH/MIPE microstructure via SEM

3.6.1 SEM Micrographs of PolyHIPEs

The microstructure of the polyH/MIPEs was analyzed via scanning electron microscopy (SEM).The microstructures of the polyH/MIPEs are presented in Figures 15-17. Figure 15 shows the SEM micrographs of a) P7 (stabilized by as-synthesized P(AAm-co-4St)) and b) P1 (stabilized by P(AAm-co-4St + CTAB). A notable observation is the angular shape of the pores in P7, which contrasts with the more rounded pores in P1. Additionally, the pore throats of P7 are smaller in size compared to those of P1, and the pore throats of these two polyHIPE monoliths vary in size. P7 appears to have a greater number of pore throats, while P1 has fewer. The pore throats of P1 and P7 exhibit a unique morphology, with some being elongated or interconnected with other pore throats, forming a large pore throat. A thorough examination of the SEM micrographs reveals that the polyHIPEs P1-P3 (stabilized by P(AAm-co-4St + CTAB)) and P7-P8 (stabilized by as-synthesized P(AAm-co-4St)) manifest open porous microstructures, characterized by interconnected pores. A noteworthy observation is depicted in Figure 16a, where a thin layer of

polymer appears to envelop the pore throats. This phenomenon may be attributed to the thin film that encloses the internal phase becoming torn as it is removed during the drying process due to the change in volume/shrinkage of the polyHIPE.[43] The SEM micrographs reveal that the polyHIPEs P1-P3 (stabilized by P(AAm-co-4St + CTAB)) and P7-P8 (stabilized by as-synthesized P(AAm-co-4St)) exhibit open porous microstructures with interconnected pores, suggesting a uniform morphology across all polyHIPEs. While there is variation in the pore size among the monoliths, the micrographs consistently demonstrate a substantial number of pore throats within the polyHIPEs. It is noteworthy that, except for P1, the pore throats appear to be of a similar size, suggesting a random distribution.

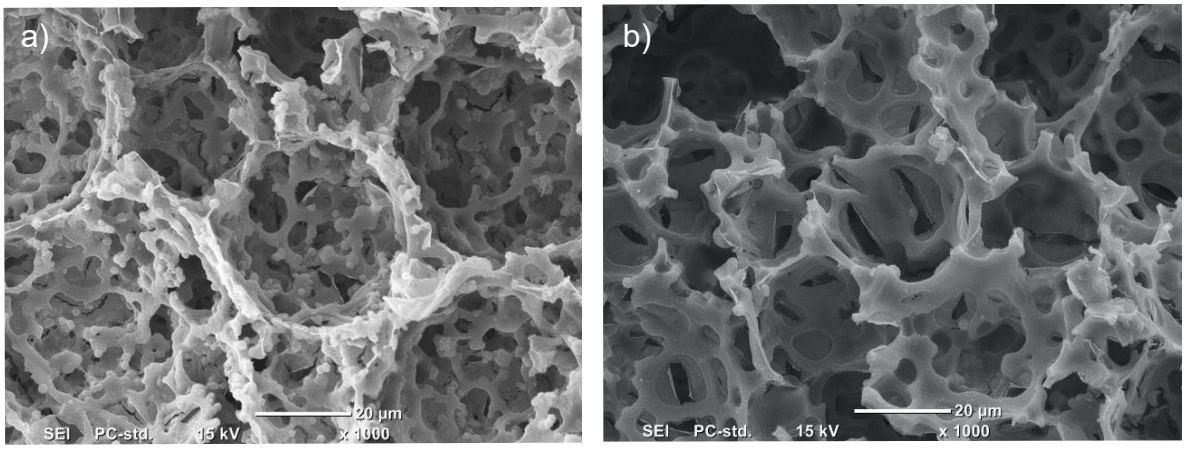

Figure 15 – SEM micrographs of a) P7 (stabilized by as-synthesized P(AAm-co-4St)) and b) P1 (stabilized by P(AAm-co-4St + CTAB)

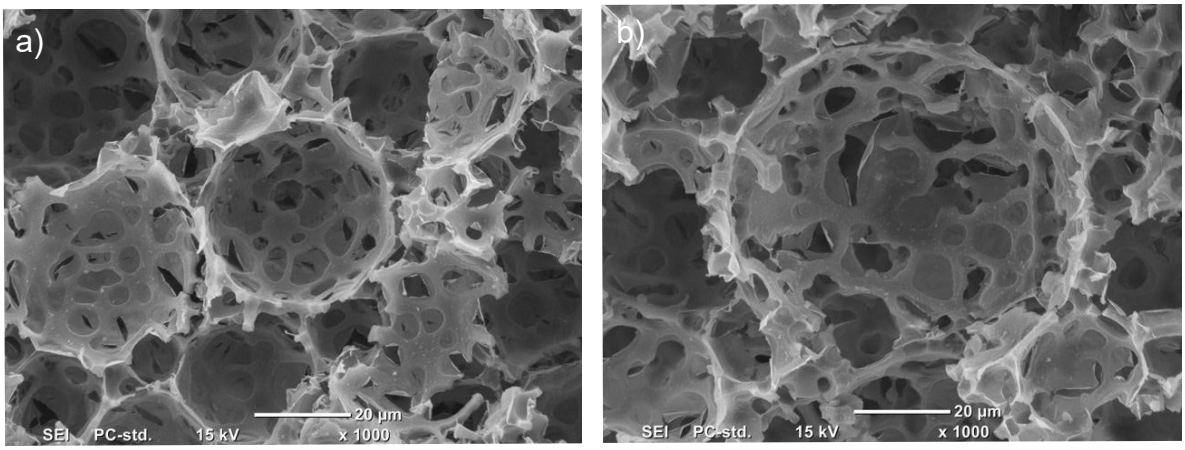

Figure 16 - SEM micrographs of a) P8 (stabilized by as-synthesized P(AAm-co-4St) and b) P2 (stabilized by P(AAm-co-4St + CTAB)

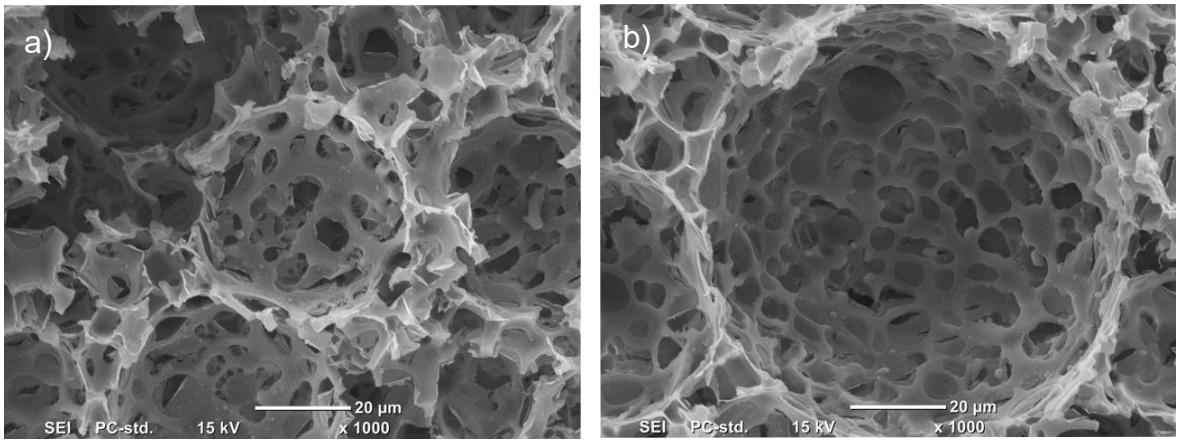

Figure 17 – SEM micrographs of a) P9 (stabilized by as-synthesized P(AAm-co-4St) and b) P3 (stabilized by P(AAm-co-4St + CTAB)

3.6.2 SEM Micrographs of PolyMIPEs

In addition to polyHIPEs, polyMIPEs (Figures 18-20) were produced. Like the polyHIPEs, the polyMIPEs exhibited an interconnected and open-porous structure. PolyMIPEs derived from MIPEs stabilized by P(AAm-co-4St + CTAB) are seen in Figure 18c and b. It is notable that these polyMIPEs possess some quite large pores, larger than those of the same polyMIPE which was produced from MIPE stabilized by as-synthesized P(AAm-co-4St). The pore size varies, with large pores found adjacent to comparatively small pores. Figure 18c shows a close-up of a single pore, illustrating a clear hierarchy. The pore is large, with the pore throats dividing into groups of smaller and larger throats. The distribution of these throats does not appear to be random. In contrast, the polyMIPEs produced from MIPEs stabilized by as-synthesized P(AAm-co-4St) (see Figure 18a and d) exhibit a different morphology. In these micrographs, the distinction between pores and pore throats is not readily apparent. However, it is noteworthy that all visible pores exhibit a comparable size, a characteristic that is equally observed in the pore throats. In contrast to the monoliths produced with P(AAm-co-4St + CTAB), no discernible hierarchy is observed in the size of the pore throats. Instead, they appear to be distributed randomly. A notable observation is the presence of globular structures within the pores and, to a lesser extent, within the pore throats. These structures may ultimately stem from larger polymer aggregates. The broad distribution of pore size in monoliths produced with as-synthesized P(AAm-co-4St) can be attributed to the reduced quantity of CTAB. According to elemental analysis, 0.01 wt.% of CTAB was still associated to the as-synthesized polymer. This means $2.74 \cdot 10^{-4}$ mol/L of CTAB are

present in the HIPE. In the HIPEs where CTAB was added, 0.1 wt.% of CTAB was added, resulting in a final concentration of $2.74 \cdot 10^{-3}$ mol/L, which is higher by a factor of 10. Therefore, the addition of CTAB and the overall concentration of CTAB greatly affects not only the pore size itself, but also the distribution of pore throats, resulting in the formation of a hierarchy.[44] Similar findings for the pore- and pore throat dimensions are observed for polyMIPEs in Figures 19 and 20 for P4, P5, P6, P10, P11 and P12. The SEM micrographs of the polyH/MIPEs were subsequently analyzed to quantify the number of pores and determine the dimensions of the pores and the width of the pore throats.

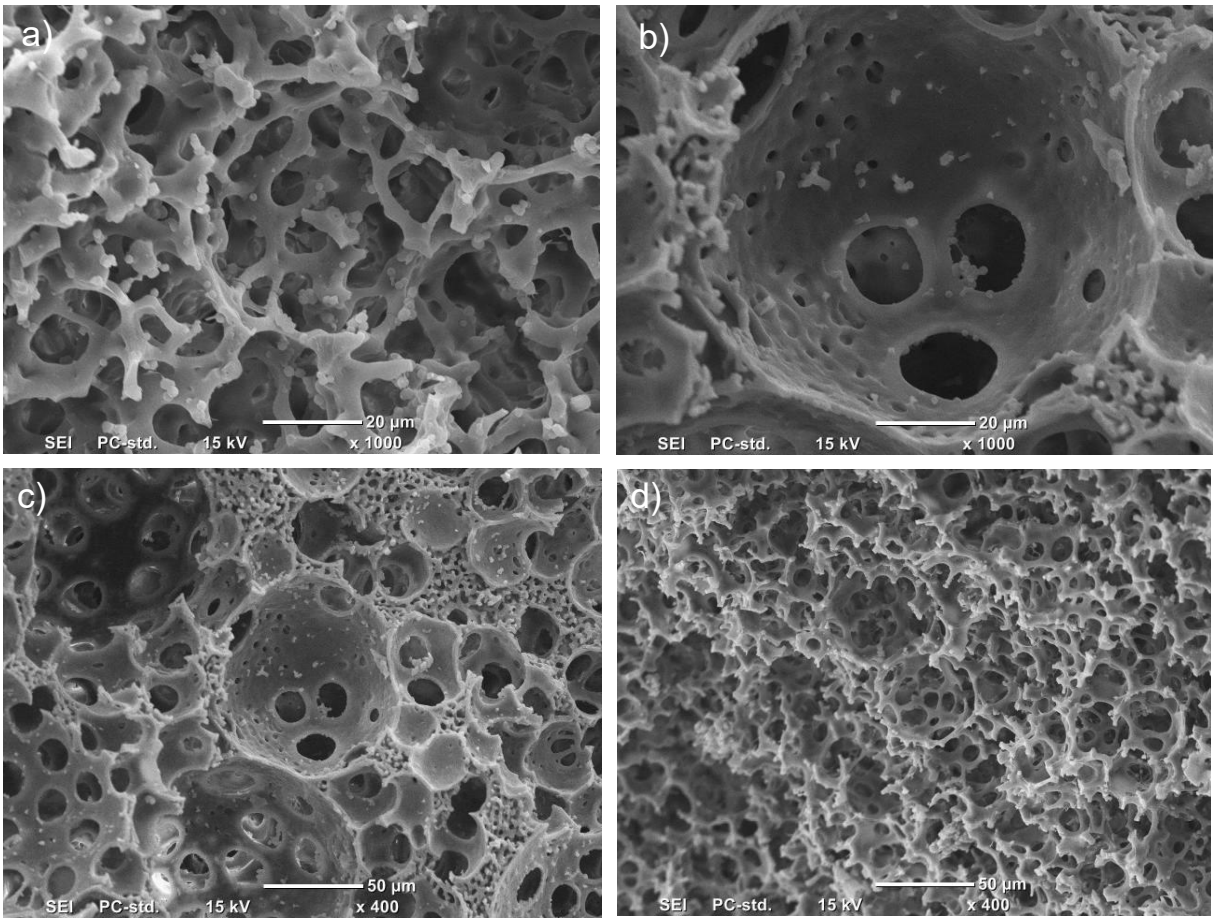

Figure 18 – SEM micrographs of a) and d) P10 (stabilized by as-synthesized P(AAm-co-4St)), c) and b) P4 (stabilized by P(AAm-co-4St + CTAB)

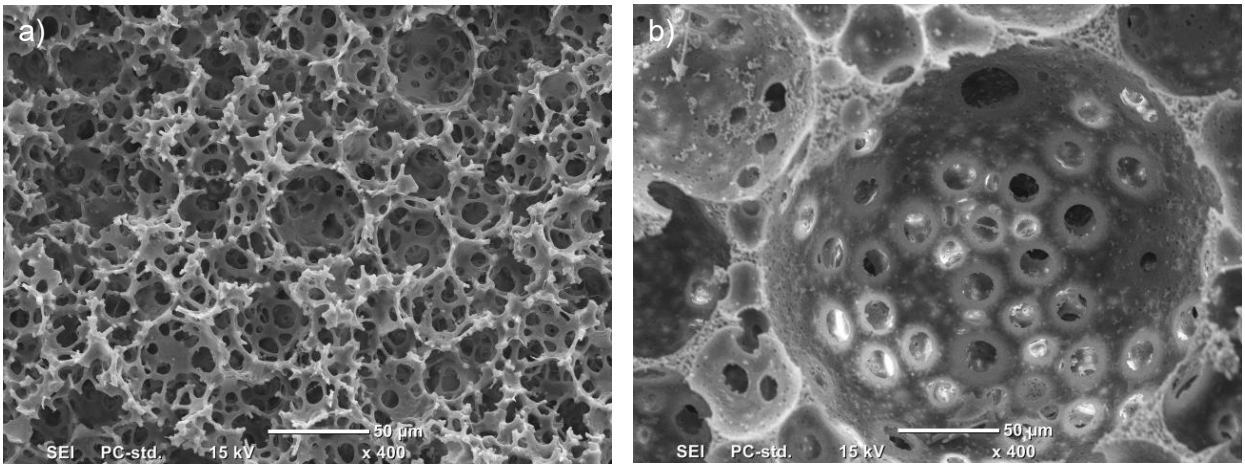

Figure 19 – SEM micrographs of a) P11 (stabilized by as-synthesized P(AAm-co-4St)) and b) P5 (stabilized by P(AAm-co-4St + CTAB)

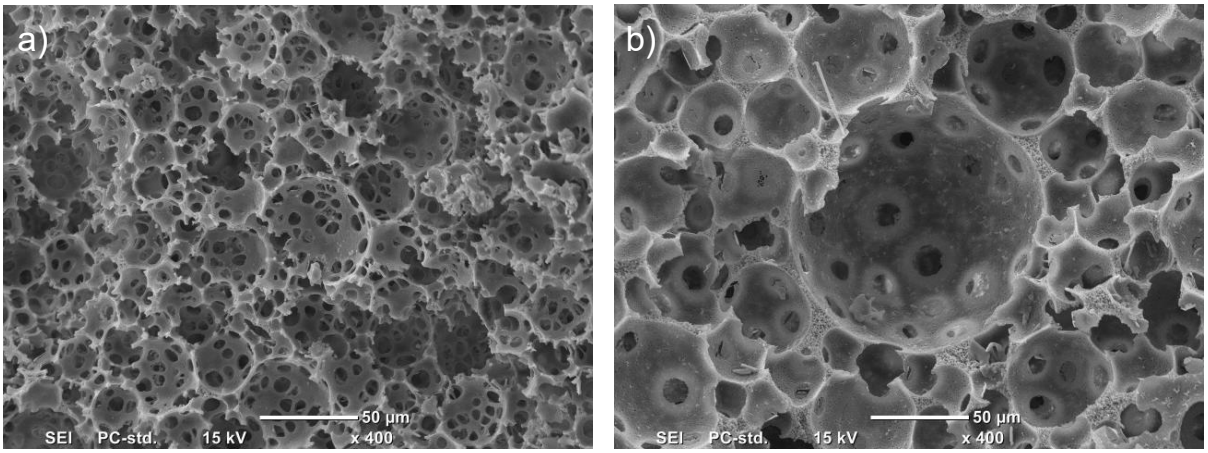

Figure 20 - SEM micrographs of a) P12 (stabilized by as-synthesized P(AAm-co-4St)) and b) P6 (stabilized by P(AAm-co-4St + CTAB))

3.6.3 Dimensions of Pores and Pore Throats

The diameter of the pores and pore throats was evaluated. The results are presented in Table 5. Samples P1-P3 were stabilized by purified P(AAm-co-4St) and CTAB. Samples P7-P9 and P7'-P9' were stabilized by as-synthesized P(AAm-co-4St). The aforementioned samples are polyHIPEs. Samples P4-P6 and P10-P12 are polyMIPEs. P4-P6 were stabilized by purified P(AAm-co-4St) and CTAB, while P10-P12 were stabilized by as-synthesized P(AAm-co-4St). In the polyHIPE group, the samples stabilized by purified P(AAm-co-4St) and CTAB exhibit pore diameters, ranging from 10 to 25 μm. Additionally, the pore throat diameters are consistent and in a range of 6-7 µm. In the case of P9-P7, the pore diameters fall within the range of 25-31 µm. For P7'-P9', the pore diameters vary between 90 and 150 µm. This observation may be attributed to the fact that P7'-

P9' were stabilized by as-synthesized P(AAm-co-4St) with a concentration of 0.1 wt.%, whereas P7-P9 was stabilized with a concentration of 0.15 wt.%, to see if a higher amount of polymer leads to changes in porosity and mechanical properties. An increased concentration of polymer results in a higher number of polymer molecules accumulating at the interface between the oil and water phase. A higher concentration of polymer at the interface is expected to facilitate the formation of droplets by reducing the interfacial tension. This prevents the droplets from merging. The original size of the droplets in the HIPE directly influences the size of the pores in the resulting polyHIPE. Consequently, the formation of smaller pores can be observed in the polyHIPEs. The pore throats are relatively similar in size and comparable to the pore throat diameter of P1-P3. A similar pattern is observed for the polyMIPEs. P4-P6 exhibit a pore diameter of 36-52 µm and slightly larger pore throat diameters in comparison to the polyHIPEs, which range from 11-14 µm. In contrast, polyMIPEs P10-P12 exhibit a smaller pore diameter, with a range of 26-29 µm. The pore throat diameters of P10-P12 are lower, with a range of 5-8 µm. In general, it can be concluded that the polyHIPEs originating from HIPEs which were stabilized with purified P(AAm-co-4St) and CTAB exhibited a smaller and more uniform pore and pore throat diameter than those samples stabilized by as-synthesized P(AAm-co-4St). In the case of the polyHIPEs that were stabilized using as-synthesized P(AAm-co-4St), a greater range of pore diameters was observed. This may be due to an unequal distribution of residual CTAB associated with the polymer after synthesis. In the case of the purified P(AAm-co-4St), a fixed quantity of CTAB was added to the stock solution, resulting in a final concentration of 0.1 wt.% CTAB in the polyHIPE. In general, the polyHIPEs derived from HIPEs stabilized by purified P(AAm-co-4St) and CTAB tend to exhibit a smaller pore diameter for the HIPEs.

Table 5 – Pore diameter d_p and pore throat diameter d_{pt} of samples P1-P12 and P7'-P9'

Sample	d_p [µm]	d_{pt} [µm]
P1	21 ± 12	7 ± 2
P2	25 ± 13	7 ± 3
P3	20 ± 10	6 ± 2
P4	50 ± 31	14 ± 4
P5	52 ± 33	11 ± 3
P6	36 ± 19	12 ± 4
P7	31 ± 14	7 ± 3
P8	28 ± 9	6 ± 2
P9	25 ± 10	6 ± 2
P7'	110 ± 50	7 ± 2
P8'	150 ± 70	6 ± 2
P9'	90 ± 40	6 ± 2
P10	29 ± 10	8 ± 3
P11	29 ± 9	7 ± 2
P12	26 ± 12	5 ± 2

3.7 Skeletal Density and Porosity of polyH/MIPE Monoliths

In Table 6, the data for the skeletal density (ρ_s), foam density (ρ_f) and porosity of the analyzed samples is shown. The polyHIPEs P1-P3 were found to have skeletal densities of 1372 ± 47 kg/m³, 1362 ± 37 kg/m³, and 1362 ± 33 kg/m³, respectively. All three samples reached porosity of 90%. The densities of P7-P9 and P7'-P9' are comparatively lower. P7, P8 and P9 have skeletal densities of 1344 ± 26, 1309 ± 58 and 1343 ± 22 kg/m³, which showed minimal variation. P7', P8' and P9' have lower skeletal densities than P7-P9, namely of 1284 ± 20, 1287 ± 15 and 1296 ± 16 kg/m³. Just like P7-P9, P7'-P9' also show a rather minimal variation of the skeletal density. Like P1-P3, the porosity of the samples P7-P9 also reached 90%. In the case of samples P7'-P9', the porosity is observed to decrease slightly, reaching values between 85 and 90%. P4, P5 and P6 are polyMIPEs, which reached skeletal densities of 1292 ± 4, 1295 ± 4 and 1300 ± 8 kg/m³. These values are lower than those observed for the comparable polyHIPEs, P1-P3. PolyMIPEs are synthesized a with lower internal phase ratio (58.6:41.4) than the polyHIPEs (70.1:29.9), meaning they contain less dispersed phase. The polyMIPEs P10-P12 have a comparable density of 1290–1308 kg/m³. The porosity is within the range of 86-87%. PolyHIPEs (P7-P9 und P7'-P9') exhibit a porosity of up to 90%, while polyMIPEs demonstrate a porosity of 86-87%. The foam density of polyHIPEs synthesized from emulsions stabilized with purified P(AAm-co-4St) and CTAB (P1-P3) the foam density ranges between 137 and 139 kg/m³. These values are relatively constant. In

contrast, polyHIPEs synthesized from emulsions stabilized as-synthesized P(AAm-co-4St) (P7-P9 and P7'-P9') exhibit foam densities between 125 and 153 kg/m^3. They show a greater variability, suggesting an uneven distribution of the pores. This finding is consistent with the results for the skeletal density. A possible explanation for this occurrence is, that the amount of CTAB which stays associated to the polymer after synthesis is inconsistent, leading to a greater variability in the results. The purified P(AAm-co-4St) and CTAB, a more narrow distribution of the density is found. The polyMIPEs however show significantly higher foam densities. The polyMIPEs synthesized from emulsions stabilized by purified P(AAm-co-4St) and CTAB (P4-P6) exhibit foam densities from 190 to 200 kg/m^3. PolyMIPEs synthesized from emulsions stabilized by as-synthesized P(AAm-co-4St) (P10-P12) have slightly lower foam densities compared to those polyMIPEs which were synthesized from emulsions stabilized by purified P(AAm-co-4St), with densities ranging from 176 and 180 kg/m^3.

Table 6 – Skeletal density ρ_s, foam density ρ_f, and porosity of all samples, measured by pycnometry.

Sample	ρ_s [kg/m^3]	ρ_f [kg/m^3]	P [%]
P1	1372 ± 47	138 ± 23	90 ± 2
P2	1362 ± 37	139 ± 27	90 ± 2
P3	1362 ± 33	137 ± 11	90 ± 1
P4	1292 ± 4	190 ± 10	85 ± 1
P5	1295 ± 4	200 ± 24	85 ± 2
P6	1300 ± 8	197 ± 14	85 ± 1
P7	1344 ± 26	140 ± 21	90 ± 2
P8	1309 ± 58	140 ± 13	90 ± 2
P9	1343 ± 22	153 ± 17	90 ± 1
P7’	1284 ± 20	136 ± 3	85 ± 3
P8’	1287 ± 15	125 ± 9	87 ± 3
P9’	1296 ± 16	131 ± 6	90 ± 2
P10	1292 ± 4	176 ± 15	86 ± 1
P11	1290 ± 12	180 ± 13	86 ± 1
P12	1308 ± 20	178 ± 6	87 ± 1

3.7 Swelling Capacity of HEMA/MBAm PolyH/MIPEs

Figure 21a illustrates the water swelling ratio (Q) as a function of time. The swelling ratio represents by how much the material increases in size after absorbing liquid. It is expressed relative to its initial state. The swelling capacity in contrast is defined as the maximum amount of liquid the material can absorb until it is fully saturated. In this series of experiments, the swelling capacity of polyHIPEs and polyMIPEs was determined. The samples previously

underwent compression tests. For purposes of comparison, the swelling capacities of the original, uncompressed samples have been included in the plot. The data indicates that all the tested samples reach a comparable swelling level within approximately 2 h. The values then stabilize at Q≈8 to Q≈10, indicating that the samples absorb water rapidly and then remain in equilibrium state. No significant difference is observed between the previously compressed samples and the original samples. Similarly, no significant difference is found when comparing the sample groups P8, P8', and P11. These findings suggest that compression testing did affect the polyH/MIPEs their swelling capacity. Figure 21b presents a plot of the equilibrium swelling capacity (Q_E) of polyH/MIPEs as a function of the cross-linking monomer concentration (MBAm) in mol%. The polyHIPE samples have been divided into two groups, "P7 - P9" and "P7' - P9'," while the polyMIPEs are classified as "P10 - P12." In general, the equilibrium swelling capacity (Q_E) of the samples was found to be inversely correlated with the MBAm content of the polyH/MIPEs. The equilibrium swelling capacity (Q_E) decreased with higher concentration of the cross-linking monomer (MBAm). At lower concentrations of the cross-linking monomer (14-16 mol%), the swelling capacity is reaching a maximum, with values approaching Q_E ≈10 for all the tested groups. A reduction in cross-link density results in a polymer network of reduced density, which is capable of expansion. This enables the tested polyHIPEs to absorb a greater quantity of water.[45] An increase in the concentration of MBAm to 18-24 mol% was observed to result in a reduction in the swelling capacity, Q_E. This finding suggests that a higher concentration of MBAm limits the ability of polyH/MIPE to swell, as a structure with a higher degree of cross-linking is less permeable to water molecules than a less cross-linked structure. Consequently, the water uptake capacity of the polyH/MIPEs is constrained.[46] The polyHIPEs designated "P7-P9" and "P7'-P9'" exhibit a comparable swelling capacity, with minimal variation. In contrast, the polyMIPEs P10-P12 show a reduced swelling capacity at the corresponding concentration of MBAm. These findings suggest that structural differences between polyHIPEs and polyMIPEs are responsible for the observed variation in water retention capacity. The polyMIPEs were observed to show a reduced capacity for swelling, compared to the polyHIPEs under identical experimental conditions.

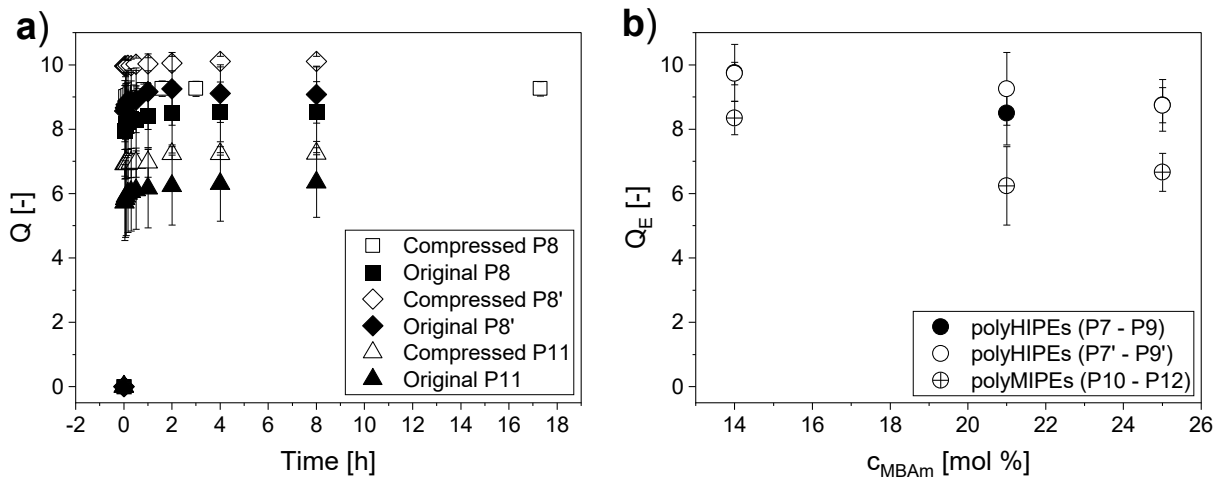

Figure 21 – a) The swelling ratio Q as a function of time and b) equilibrium water swelling ratio Q_E as a function of the MBAm content

3.8 Mechanical Properties of Swollen PolyH/MIPEs

Figure 22 a-f shows the stress-strain curves of swollen monolithic polyH/MIPEs. Loading, unloading, and reloading cycles were carried out. The samples prepared from high internal phase emulsions (HIPEs) are E8 and E8'. The medium internal phase emulsion (MIPE) is E11. Both of these emulsions were stabilized by as-synthesized P(AAm-co-4St). Two types of samples were included: undamaged, swollen hydrogels and those that were previously subjected to compression tests and then re-swollen. Figure 22a shows the stress-strain curve for the undamaged and swollen polyHIPE (P8). The curve indicates that energy is being dissipated in the material. During reloading, polyHIPE can sustain stress, although the curve is shifted to lower stress values than the initial loading curve. These results suggest that plastic deformation of the polyHIPE is taking place. Figure 22b shows P8, which has been previously compression loaded and re-swollen. The stress level during loading and reloading is significantly lower than for the undamaged P8. This reduction suggests that the initial compression has damaged the polyHIPE structure and reduced its resistance to compression load. A smaller hysteresis loop is found for the previously compression loaded P8. This finding indicates a reduced capacity for energy dissipation. This is probably due to structural damage, limiting the stress resistance of the polyHIPEs. Figure 22c shows the stress-strain curve of undamaged and swollen polyHIPE P8'. This curve is very similar to that of P8. It also shows a hysteresis loop and stress retention during reloading. Figure 22d shows the previously compression loaded and re-swollen P8'. A decrease

in the maximum stress capacity of the material can be seen when comparing the curve with that of the undamaged and swollen P8' in Figure 22c. Again, the hysteresis loop is smaller. This indicates, that the polyHIPE has lost some of its elastic behaviour due to previous damage. Figure 22e shows the undamaged and swollen polyMIPE. Compared to the polyHIPEs, the polyMIPE shows increased stress at each corresponding strain. This indicates that the polyMIPEs have a higher stiffness in the original and undamaged state. The polyMIPE shows a greater hysteresis, indicating that there is a high energy dissipation during deformation. This means that the polyMIPE may be more stress resistant than the polyHIPEs tested. Figure 22f shows the pre-compressed and re-swollen polyMIPE. The pre-compression reduces the stress resistance, elasticity, and energy dissipation of polyMIPEs. Damaged samples exhibit lower stress values, smaller hysteresis loops, and irreversible structural changes due to plastic deformation. The tested PolyMIPEs generally display higher initial stiffness compared to the tested polyHIPEs.

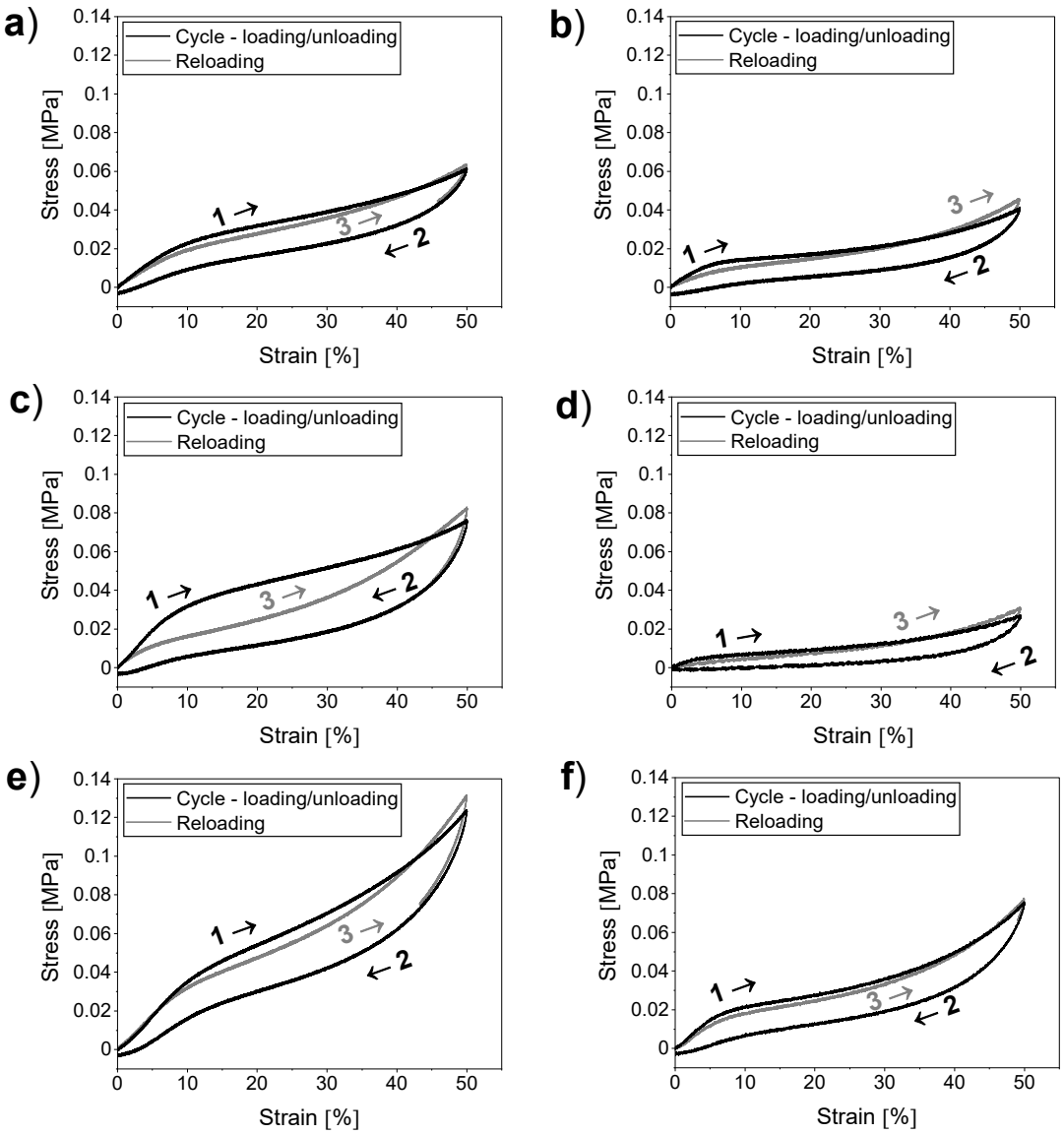

Figure 22 – Stress-strain curves from loading/unloading and reloading cycles of polyHIPEs a) P8, b) precompressed P8, c) P8', d) precompressed P8'and polyMIPEs e) polyMIPE and f) precompressed polyMIPE

3.9 Impact of the Styrene Moieties on the Foaming Properties of P(AAm-co-St)

Figure 23 presents initial experiments, which were conducted to produce foam. In these experiments, the following samples were used: P(AAm-co-St) with two different styrene contents and the polyacrylamide homopolymer, which served as the control sample. The concentrations were varied between 100 and 3000 ppm. It is evident that the polyacrylamide homopolymer exhibits the lowest capacity for foaming among the tested samples. At lower concentrations of 100–1000 ppm, minimal foaming was observed. At the highest concentration tested (3000 ppm),

foaming was observed, with a layer of foam forming on the surface of the solution. However, the resulting foam exhibited larger bubbles and produced less foam than that observed for P(AAm-co-2St) and P(AAm-co-4St) at 3000 ppm. P(AAm-co-2St) and P(AAm-co-4St) demonstrated superior foaming properties. At the highest concentration of 3000 ppm, a greater quantity of foam was observed for P(AAm-co-4St), nearly twice that of P(AAm-co-2St). Therefore, P(AAm-co-4St) was selected for all subsequent experiments.

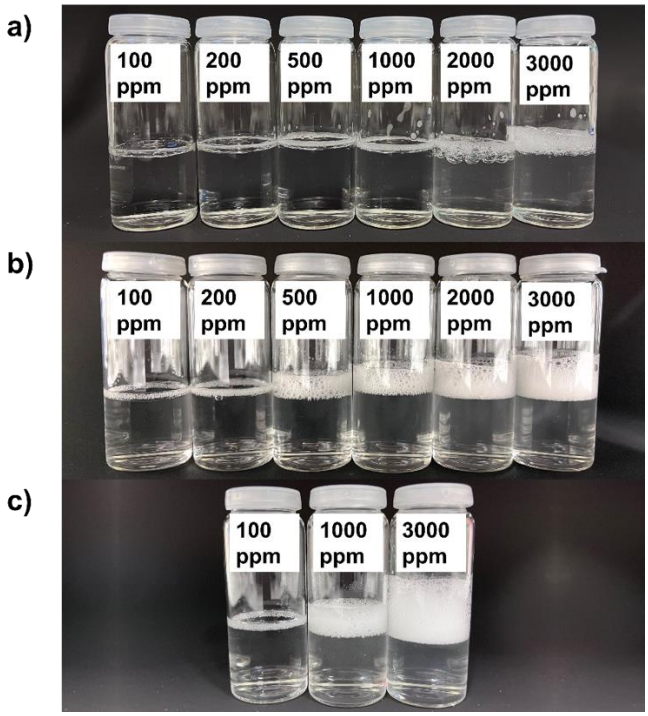

Figure 23 – Aqueous solutions, shaken by hand to produce foam with concentrations ranging from 100-3000 ppm of a) polyacrylamide homopolymer b) P(AAm-co-2St) c) P(AAm-co-4St)

3.10 Microstructure of Air-dried Foam

The foam stabilized by the as-synthesized P(AAm-co-4St) was collected from the ViEDRA tank and subsequently air-dried. This process was relatively straightforward, as the foam did not collapse, and no shrinkage was observed. The foam was observed to be free-standing and exhibited no signs of damage. Figures 24a and b present scanning electron microscopy (SEM) micrographs of the air-dried foam. Many of the foam cells were found to be coated with a polymer film after air-drying. The foam cells are relatively large and do not appear to be interconnected. Micrographs of the freeze-dried foam are illustrated in Figures 24c and d. In contrast to the air-dried foam,

the freeze-dried foam exhibited a denser structure, with signs of collapse in certain areas. A comparison of the micrographs of the air-dried and freeze-dried foams reveals the absence of the polymer film, which was observed for the air-dried foam. Additionally, the freeze-dried foam appears to have smaller cells. This might be due to the foam undergoing shrinkage during the freeze-drying process. Figure 24a provides a macroscopic comparison of the fresh foam as collected from ViEDRA. Figure 24b depicts a section of freeze-dried foam, while Figure 24c shows the air-dried foam.

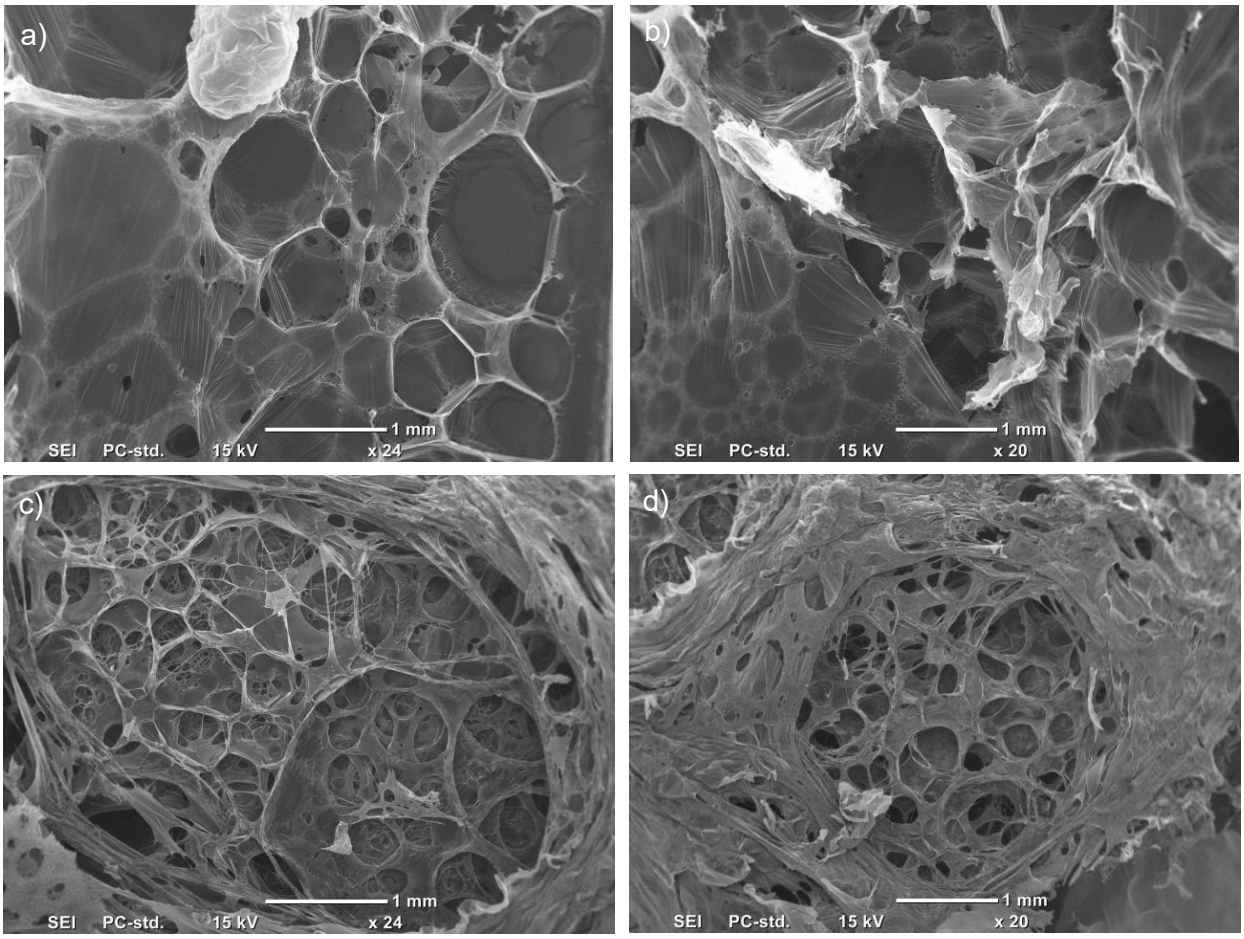

Figure 24 – SEM Micrographs of P(AAm-co-4St) foam, derived from 0.1M NaCl solution a), b) air-dried section of foam and c), d) freeze-dried section of foam

As illustrated in Figure 25, the P(AAm-co-4St) foam, derived from a 0.1M NaCl solution in the ViEDRA, exhibits distinct characteristics. Figure 25a depicts the immediate state of the foam after its harvesting from the ViEDRA tank, showing a gelatinous consistency. Most of the air is encapsulated within smaller bubbles. There are some larger bubbles that collapsed during the drying

process, both in the air and to some extent within the freeze-dryer. In Figure 25b, a section of freeze-dried foam is shown. The foam exhibited a soft and sponge-like texture. Figure 25c depicts a section of air-dried foam. In contrast to the freeze-dried foam, the air-dried foam appears to be less collapsed. The larger size of the bubbles and the overall difference in consistency, characterized by a higher degree of rigidity in the air-dried foam compared to the freeze-dried foam, might be attributed to the higher drying rate of the freeze-dried foam in the freeze dryer. The slower drying process of air-drying leads to more bubbles collapsing into larger structures.

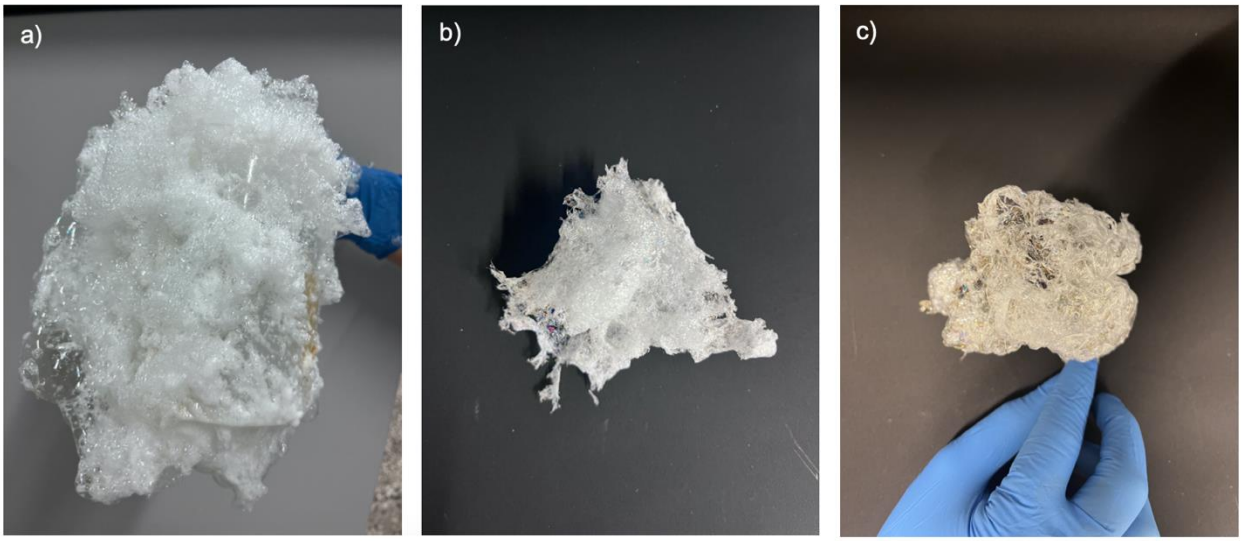

Figure 25 – P(AAm-co-4St) foam, obtained from 0.1M NaCl solution in the ViEDRA a) fresh foam, immediately after harvesting the foam from the ViEDRA tank b) a section of freeze-dried foam and c) a section of air-dried foam

3.11 Removal of P(AAm-co-4St) from Aqueous Solution

Figure 26a illustrates the molecular weight distribution of P(AAm-co-4St) in aqueous NaCl solution from the ViEDRA, as well as of the re-dissolved foam. The normalized weight fraction of P(AAm-co-4St) is presented as a function of the molecular weight (M_w). The blue curve represents the aqueous solution of P(AAm-co-4St) that remained in the ViEDRA after a specified number of cycles. The black curve represents the extracted P(AAm-co-4St) from the foam. A comparison of the two curves reveals that the foaming affects the distribution of molecular weight, which results in a shift towards higher molecular weights in the foam. This suggests that the foaming of P(AAm-co-4St) resulted in an enrichment of fractions with higher molecular weights. These observations may be explained by the greater intramolecular interactions exhibited by chains of

higher molecular weight, which contribute more significantly to the formation of foam. In contrast, shorter chains raise the viscosity of solutions to a smaller extent, contributing lesser to the stability of the foam structure. Additionally, the affinity of the chains for the interface may contribute to the enrichment of chains of higher molecular weight in the foam. Chains of higher molecular weight may have a stronger tendency to accumulate at the air/water interface.[47] 26b shows the detector signal in mV as a measure off the refractive index as a function of retention volume of P(AAm-co-4St) solutions. The solutions were collected from the ViEDRA by taking samples at various time points. The curves show that the polymer concentration in solution decreases from 174 ppm to 78 ppm. This underlines the gradual reduction of P(AAm-co-4St) in the ViEDRA tank over time, as the polymer is extracted stepwise as foam meaning the polymer is retained in the foam. Higher retention volumes correlate to lower concentrations, which indicates that a steady decrease of P(AAm-co-4St) in the ViEDRA. Overall, the data clearly shows that the foaming greatly impacts the distribution of the molecular weight and the concentration of P(AAm-co-4St) in the solution.

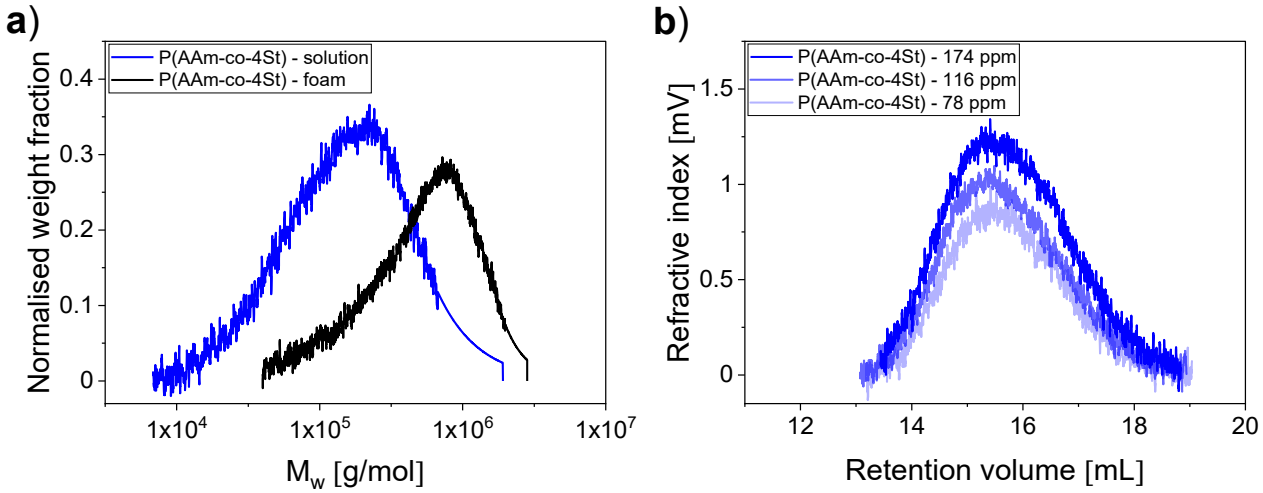

Figure 26 - Molecular weight distribution of P(AAm-co-4St) in the solution and of the re-dissolved foam measured by the GPC of a) the normalized weight fraction as a function of M_w and b) the refractive index as a function of the retention volume

3.12 Liquid Foam Properties

Figure 27 presents the results of the foam analyzer measurements, which show the stability of the P(AAm-co-4St) foam over time. The data includes the foam volume, liquid content, bubble count, and bubble area. The foam which was used in these experiments was extracted from the ViEDRA tank, which contained an aqueous 0.1M NaCl P(AAm-co-4St) solution. Figure 27a illustrates the foam volume (black) and the total volume (red) as a function of time in hours. At the onset, both volumes are relatively high. Initially and up to 4h, a slight reduction in both the foam and total volume is observed. However, both volumes seem to reach a plateau and remain constant over the whole measurement period. Figure 27b shows the percentage of liquid content in the foam over time. The liquid content decreases in a stepwise manner over a period of 2h. This indicates that the foam underwent drainage. Over the final 2h, the liquid content stabilizes and reaches a plateau at a lower value. The initial decrease in the liquid content happens due to the loss of solution from the foam, which resulted in a dry and mechanically more stable foam. Figure 27c presents the evolution of the bubble count and mean bubble area over time. The bubble count is represented by the green curve. The bubble count starts at a higher value but decreases over time. This is to be expected, given the fact that some of the bubbles may burst or merge with one another. Consequently, the mean bubble area, depicted as the black curve, increases with time. This can also be explained by the collapse of parts of the foam structure and the merging of bubbles. This is a typical and expected behavior of foams of all kinds.[48] However, it is noteworthy that the foam stabilizes after a period of hours.

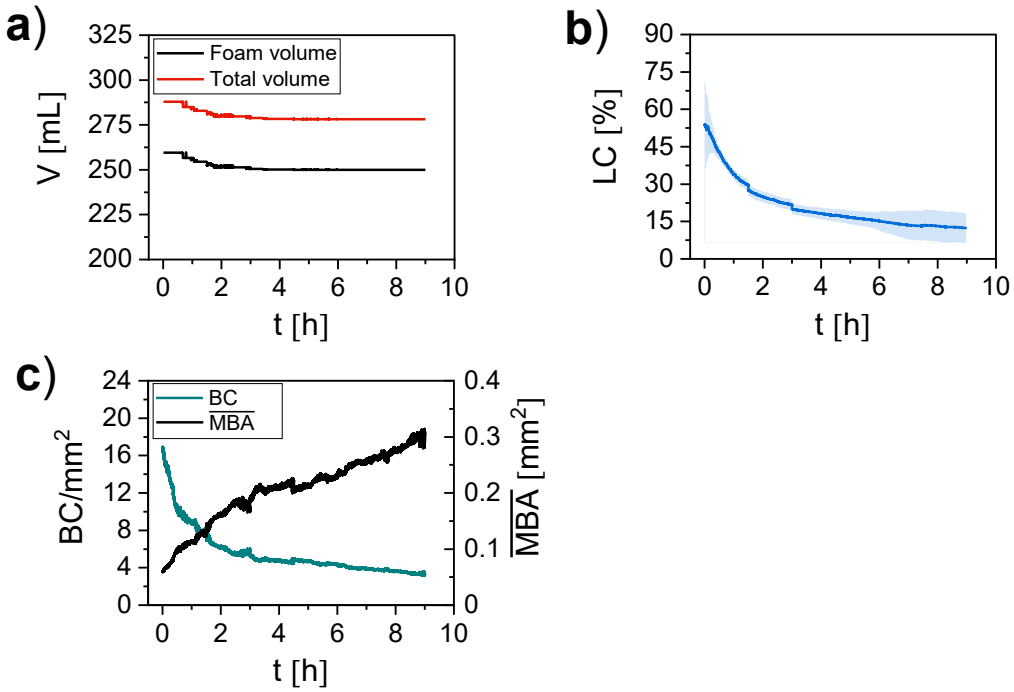

Figure 27 – Results of the measurements conducted with the foam analyzer a) foam volume and the total volume as a function of time b) percentage of liquid content in the foam over time c) bubble count per mean bubble area over time

4 Summary and Outlook

The copolymer P(AAm-co-St) has been synthesized by the addition of different amounts of styrene to vary the hydrophobic moieties. In preliminary experiments, including the production of HIPEs and the handshaking of aqueous solutions to create foam, P(AAm-co-4St) was identified as the polymer showed the most effective emulsifying and foaming properties. P(AAm-co-4St) was used in its as-synthesized or purified form. The impact of P(AAm-co-4St) on the interfacial tension between water and toluene was investigated. In these experiments, P(AAm-co-4St) was observed to significantly reduce the interfacial tension, thereby yielding highly favorable results. P(AAm-co-4St) was demonstrated to be an extremely effective macrosurfactant, capable of reducing the interfacial tension to a value that was lower than that achieved with CTAB alone. The combination of purified P(AAm-co-4St) with externally added CTAB resulted in a highly efficient reduction of the interfacial tension. Accordingly, two series of polyH/MIPEs were produced, utilizing the purified P(AAm-co-4St) in conjunction with 0.1 wt.% CTAB and the as-

synthesized P(AAm-co-4St), which had CTAB associated from the synthesis. The two variants of the polymer were observed to produce HIPEs at a low concentration of macrosurfactant (0.1-0.15 wt.%), a result that is very favorably compared to the results reported in the literature.[42] Following the successful production of emulsions, they were polymerized. A series of HEMA/MBAm-based porous monoliths was produced. Scanning electron microscopy (SEM) analysis revealed the presence of macropores and mesopores, which were partially interconnected. However, no significant difference was identified between polyH/MIPEs stabilized by purified P(AAm-co-4St) in combination with 0.1 wt.% CTAB and the as-synthesized P(AAm-co-4St). A comparison of the microstructures of polyHIPEs and polyMIPEs reveals a minimal difference, with polyMIPEs exhibiting a lower number of pore throats. The polyHIPEs exhibited a higher density and porosity in general than the polyMIPEs. This phenomenon can be attributed to the fact that polyHIPEs comprise a higher proportion of the internal phase, which consequently leads to an elevated porosity of the polyHIPE. PolyMIPEs exhibit a lower percentage of internal phase, which results in a reduction of both porosity and density. The swelling capacity was found to be limited by the higher amount of MBAm used as the crosslinking monomer. No significant difference was observed in the swelling ratio between polyHIPEs and polyMIPEs. All samples, irrespective of whether they were polyHIPEs or polyMIPEs, exhibited a gradual increase in stress with strain during the loading phase. Subsequently, a reduction in stress was observed during the unloading phase, resulting in the formation of a hysteresis loop. This suggests that energy is dissipated within the material. The reloading curve was observed to be shifted from the loading curve, indicating that plastic deformation of the polyH/MIPEs had occurred. The polyMIPE, however, exhibited superior stiffness compared to the polyHIPEs that were tested. This can be explained by the lower porosity of the polyMIPEs, which leads to an increased stiffness of the monolith.

The probing of the foaming of P(AAm-co-St) by handshaking demonstrated that the homopolymer showed the lowest capacity for foaming. The addition of 2 and 4 mol% of styrene to P(AAm-co-St) resulted in a higher capacity for foaming. It was clearly observed that P(AAm-co-4St) produced the most foam, especially when directly compared to the other samples. The foam used in the subsequent experiments was derived from the ViEDRA, produced upon pumping cycles, which caused removal of the polymer from the solution in the tank. Subsequently, the

foam was subjected to air-drying and freeze-drying. Both methods yielded stable dry foams with variations in their microstructure, as determined by scanning electron microscopy. The analysis of the molecular weight distribution demonstrated that the polymer had indeed been removed from the solution in the ViEDRA. Another important observation was that polymer chains with a higher molecular weight (~10^6 g/mol) were found to be enriched in the foam. The foam generally lost liquid volume during the first two hours; however, after a certain time, the foam structure stabilized, and the foam volume remained constant.

In conclusion, the co-polymer P(AAm-co-4St) has been demonstrated to be an extremely effective macrosurfactant. The production of high internal emulsions was successfully achieved using a minimal quantity of P(AAm-co-4St), in comparison to the amount of small molecule surfactant used in previous literature.[42] PolyHIPEs and polyMIPEs with predictable and consistent densities and porosities were successfully produced. P(AAm-co-4St) was successfully employed to produce foam and was subsequently recovered from an aqueous solution. These outcomes are promising, as polyacrylamide is quite frequently used in fracking. The potential for a polymer to be recovered and reused in fracking could prove very valuable for to the industry. The removal of the polymer could ease the treatment of wastewater. The separation properties of polyHIPEs could be used for further experiments, for instance to determine their efficiency of separating liquid/liquid mixtures. The polyHIPEs exhibited swelling behavior, making them potential candidates for applications in wound healing and soft tissue engineering. For this application, it is important to note that the HEMA/MBAm based polyHIPEs are not biodegradable. Further experiments in this field could be conducted. One potential issue with the use of polyHIPEs in the medical field is the possible presence of acrylamide, which is the monomer used for the P(AAm-co-St) synthesis. Further experiments could include the determination of residual acrylamide and the development of secure purification methods.

5 Bibliography

1) El-Ghoul, Y., Alminderej, F. M., Alsubaie, F. M., Alrasheed, R. & Almousa, N. H. (2021). Recent Advances in Functional Polymer Materials for Energy, Water, and Biomedical Applications: A Review. Polymers, 13(24), 4327. https://doi.org/10.3390/polym13244327

2) Feng, H., Lu, X., Wang, W., Kang, N. & Mays, J. W. (2017). Block Copolymers: Synthesis, Self-Assembly, and Applications. Polymers, 9(12), 494. https://doi.org/10.3390/polym9100494

3) Zhang, X., Takegoshi, K. & Hikichi, K. (1991). Miscibility of Poly(vinyl alcohol)/Poly(methacrylic acid) and Poly(vinyl alcohol)/Poly(acrylic acid) Systems: I. High-Resolution NMR Studies in Solution. Polymer Journal, 23(2), 79–86. https://doi.org/10.1295/polymj.23.79

4) Kusters, G. L. A., Zhang, G., Chen, Z. & Suo, Z. (2023). Amphiphilic monomers bridge hydrophobic polymers and water. Soft Matter, 19(48), 9489–9495. https://doi.org/10.1039/d3sm01129a

5) Lei, L., Gohy, J., Willet, N., Zhang, J., Varshney, S. & Jérôme, R. (2004). Morphology of core-shell-corona aqueous micelles: II. Addition of core-forming homopolymer. Polymer, 45(13), 4375–4381. https://doi.org/10.1016/j.polymer.2004.04.040

6) George, S., Champagne-Hartley, R., Deeter, G., Campbell, D., Reck, B., Urban, D. & Cunningham, M. (2015). Amphiphilic Block Copolymers as Stabilizers in Emulsion Polymerization: Effects of the Stabilizing Block Molecular Weight Dispersity on Stabilization Performance. Macromolecules, 48(24), 8913–8920. https://doi.org/10.1021/acs.macromol.5b01853

7) Matras, Z., Malcher, T. & Gzyl-Malcher, B. (2007). The influence of polymer–surfactant aggregates on drag reduction. Thin Solid Films, 516(24), 8848–8851. https://doi.org/10.1016/j.tsf.2007.11.057

8) Khan, H. J., Spielman-Sun, E., Jew, A. D., Bargar, J., Kovscek, A. & Druhan, J. L. (2021). A Critical Review of the Physicochemical Impacts of Water Chemistry on Shale in Hydraulic Fracturing

Systems. Environmental Science & Technology, 55(3), 1377–1394. https://doi.org/10.1021/acs.est.0c04901

9) surfactant (surface active agent). (2014b). In International Union of Pure and Applied Chemistry (IUPAC) eBooks. https://doi.org/10.1351/goldbook.s06194

10) Ogunmokun, F. A. & Wallach, R. (2023). Effect of surfactant surface and interfacial tension reduction on infiltration into hydrophobic porous media. Geoderma, 441, 116735. https://doi.org/10.1016/j.geoderma.2023.116735

11) Anton, P. & Laschewsky, A. (1994). Solubilization by polysoaps. Colloid & Polymer Science, 272(9), 1118–1128. https://doi.org/10.1007/bf00652381

12) Delaittre, G., Dire, C., Rieger, J., Putaux, J. & Charleux, B. (2009). Formation of polymer vesicles by simultaneous chain growth and self-assembly of amphiphilic block copolymers. Chemical Communications, 20, 2887. https://doi.org/10.1039/b903040a

13) Matsuoka, H., Suetomi, Y., Kaewsaiha, P. & Matsumoto, K. (2009). Nanostructure of a Poly(acrylic acid) Brush and Its Transition in the Amphiphilic Diblock Copolymer Monolayer on the Water Surface. Langmuir, 25(24), 13752–13762. https://doi.org/10.1021/la901466h

14) Desjardins, A. & Eisenberg, A. (1991). Colloidal properties of block ionomers. 1. Characterization of reverse micelles of styrene-b-metal methacrylate diblocks by size-exclusion chromatography. Macromolecules, 24(21), 5779–5790. https://doi.org/10.1021/ma00021a009

15) Khaliq, N. U., Lee, J., Kim, S., Sung, D. & Kim, H. (2023). Pluronic F-68 and F-127 Based Nanomedicines for Advancing Combination Cancer Therapy. Pharmaceutics, 15(8), 2102. https://doi.org/10.3390/pharmaceutics15082102

16) Raffa, P., Wever, D. A. Z., Picchioni, F. & Broekhuis, A. A. (2015). Polymeric Surfactants: Synthesis, Properties, and Links to Applications. Chemical Reviews, 115(16), 8504–8563. https://doi.org/10.1021/cr500129h

17) Webber, S. E. (1998). Polymer Micelles: An Example of Self-Assembling Polymers. The Journal Of Physical Chemistry B, 102(15), 2618–2626. https://doi.org/10.1021/jp980386o

18) Mok, M. M., Thiagarajan, R., Flores, M., Morse, D. C. & Lodge, T. P. (2012). Apparent Critical Micelle Concentrations in Block Copolymer/Ionic Liquid Solutions: Remarkably Weak Dependence on Solvophobic Block Molecular Weight. Macromolecules, 45(11), 4818–4829. https://doi.org/10.1021/ma300399c

19) Lee, R.-S. & Wu, K.-P. (2011). Synthesis and characterization of temperature-sensitive block-graft PNIPAAM-B-(PAN3CL-G-alkyne) copolymers by ring-opening polymerization and click reaction. Journal Of Polymer Science Part A: Polymer Chemistry, 49(14), 3163–3173. https://www.academia.edu/61761820/Synthesis_and_characterization_of_temperature_sensitive_block_graft_PNiPAAm_b_P%CE%B1N3CL_g_alkyne_copolymers_by_ring_opening_polymerization_and_click_reaction

20) Garnier, S. & Laschewsky, A. (2005). Synthesis of New Amphiphilic Diblock Copolymers and Their Self-Assembly in Aqueous Solution. Macromolecules, 38(18), 7580–7592. https://doi.org/10.1021/ma0506785

21) Zhang, J., Dubay, M. R., Houtman, C. J. & Severtson, S. J. (2009). Sulfonated Amphiphilic Block Copolymers: Synthesis, Self-Assembly in Water, and Application as Stabilizer in Emulsion Polymerization. Macromolecules, 42(14), 5080–5090. https://doi.org/10.1021/ma900795f

22) Gaudin, T., Rotureau, P., Pezron, I. & Fayet, G. (2018). Investigating the impact of sugar-based surfactants structure on surface tension at critical micelle concentration with structure-property relationships. Journal Of Colloid And Interface Science, 516, 162–171. https://doi.org/10.1016/j.jcis.2018.01.051

23) emulsion. (2014). In International Union of Pure and Applied Chemistry (IUPAC) eBooks. https://doi.org/10.1351/goldbook.e02065

24) Costa, C., Medronho, B., Filipe, A., Mira, I., Lindman, B., Edlund, H. & Norgren, M. (2019). Emulsion Formation and Stabilization by Biomolecules: The Leading Role of Cellulose. Polymers, 11(10), 1570. https://doi.org/10.3390/polym11101570

25) Muratspahić, E., Schöffmann, J., Jiang, Q. & Bismarck, A. (2023b). Poly(acrylamide- CO-styrene): a macrosurfactant for Oil/Water emulsion templating toward robust macroporous hydrogels. Macromolecules, 56(8), 3213 - 3223. https://doi.org/10.1021/acs.macromol.2c02504

26) Owen, R., Sherborne, C., Evans, R., Reilly, G. C. & Claeyssens, F. (2020). Combined Porogen Leaching and Emulsion Templating to produce Bone Tissue Engineering Scaffolds. International Journal Of Bioprinting, 6(2), 265. https://doi.org/10.18063/ijb.v6i2.265

27) Tebboth, M., Menner, A., Kogelbauer, A. & Bismarck, A. (2014). Polymerised high internal phase emulsions for fluid separation applications. Current Opinion in Chemical Engineering, 4, 114–120. https://doi.org/10.1016/j.coche.2014.03.001

28) He, H., Li, W., Lamson, M., Zhong, M., Konkolewicz, D., Hui, C. M., Yaccato, K., Rappold, T., Sugar, G., David, N. E., Damodaran, K., Natesakhawat, S., Nulwala, H. & Matyjaszewski, K. (2014b). Porous polymers prepared via high internal phase emulsion polymerization for reversible CO2 capture. Polymer, 55(1), 385–394. https://doi.org/10.1016/j.polymer.2013.08.002

29) Matras, Z., Malcher, T. & Gzyl-Malcher, B. (2007). The influence of polymer–surfactant aggregates on drag reduction. Thin Solid Films, 516(24), 8848–8851. https://doi.org/10.1016/j.tsf.2007.11.057

30) Xi, L. (2019). Turbulent drag reduction by polymer additives: Fundamentals and recent advances. Physics Of Fluids, 31(12). https://doi.org/10.1063/1.5129619

31) Matras, Z., Malcher, T. & Gzyl-Malcher, B. (2007). The influence of polymer–surfactant aggregates on drag reduction. Thin Solid Films, 516(24), 8848–8851. https://doi.org/10.1016/j.tsf.2007.11.057

32) Lumley, J. L. (1969). Drag Reduction by Additives. Annual Review Of Fluid Mechanics, 1(1), 367–384. https://doi.org/10.1146/annurev.fl.01.010169.002055

33) Hussien, O. S., Elraies, K. A., Almansour, A., Husin, H., Belhaj, A. & Ern, L. (2019). Experimental study on the use of surfactant as a fracking fluid additive for improving shale gas productivity. Journal Of Petroleum Science And Engineering, 183, 106426. https://doi.org/10.1016/j.petrol.2019.106426

34) Al-Hajri, S., Negash, B. M., Rahman, M. M., Haroun, M. & Al-Shami, T. M. (2022). Perspective Review of Polymers as Additives in Water-Based Fracturing Fluids. ACS Omega, 7(9), 7431–7443. https://doi.org/10.1021/acsomega.1c06739

35) Basedow, A. M., Ebert, K. H. & Hunger, H. (1979). Effects of mechanical stress on the reactivity of polymers: Shear degradation of polyacrylamide and dextran. Die Makromolekulare Chemie, 180(2), 411–427. https://doi.org/10.1002/macp.1979.021800215

36) Brandfellner, L., Muratspahić, E., Bismarck, A. & Müller, H. W. (2024). Quantitative description of polymer drag reduction: Effect of polyacrylamide molecular weight distributions. Journal Of Non-Newtonian Fluid Mechanics, 325, 105185. https://doi.org/10.1016/j.jnnfm.2024.105185

37) Luu, T. T. H., Jia, Z., Kanaev, A. & Museur, L. (2020). Effect of Light Intensity on the Free-Radical Photopolymerization Kinetics of 2-Hydroxyethyl Methacrylate: Experiments and

Simulations. The Journal Of Physical Chemistry B, 124(31), 6857–6866. https://doi.org/10.1021/acs.jpcb.0c03140

38) Muratspahić, E., Brandfellner, L., Schöffmann, J., Bismarck, A. & Müller, H. W. (2022). Aqueous Solutions of Associating Poly(acrylamide-co-styrene): A Path to Improve Drag Reduction? Macromolecules, 55(23), 10479–10490. https://doi.org/10.1021/acs.macromol.2c01219

39) Shah, S. K. & Bhattarai, A. (2020). Interfacial and Micellization Behavior of Cetyltrimethylammonium Bromide (CTAB) in Water and Methanol-Water Mixture at 298.15 to 323.15 K. Journal Of Chemistry, 2020, 1–13. https://doi.org/10.1155/2020/4653092

40) Bell, C. G., Breward, C. J. W., Howell, P. D., Penfold, J. & Thomas, R. K. (2007). Macroscopic Modeling of the Surface Tension of Polymer−Surfactant Systems. Langmuir, 23(11), 6042–6052. https://doi.org/10.1021/la063714h

41) Nahringbauer, I. (1997). Polymer−Surfactant Interaction As Revealed by the Time Dependence of Surface Tension. The EHEC/SDS/Water System. Langmuir, 13(8), 2242–2249. https://doi.org/10.1021/la960976i

41) Kwok, S., Botet, R., Shglabow, A. & Cabane, B. (2020). Apollonian emulsions. EPL (Europhysics Letters), 130(3), 38001. https://doi.org/10.1209/0295-5075/130/38001

42) Kulygin, O. & Silverstein, M. S. (2007). Porous poly(2-hydroxyethyl methacrylate) hydrogels synthesized within high internal phase emulsions. Soft Matter, 3(12), 1525. https://doi.org/10.1039/b711610a

43) Durgut, E., Sherborne, C., Dikici, B. A., Reilly, G. C. & Claeyssens, F. (2022). Preparation of Interconnected Pickering Polymerized High Internal Phase Emulsions by Arrested Coalescence. Langmuir, 38(36), 10953–10962. https://doi.org/10.1021/acs.langmuir.2c01243

44) Ortiz-Martínez, V. M., Gómez-Coma, L., Ortiz, A. & Ortiz, I. (2019). Overview on the use of surfactants for the preparation of porous carbon materials by the sol-gel method: applications

in energy systems. Reviews in Chemical Engineering, 36(7), 771–787. https://doi.org/10.1515/revce-2018-0056

45) Hsieh, T., Hsieh, K., Simon, G. P., Tiu, C. & Hsu, H. (1998). Effect of crosslinking density on the physical properties of interpenetrating polymer networks of polyurethane and 2-hydroxy-ethyl methacrylate-teminated polyurethane. Journal Of Polymer Research, 5(3), 153–162. https://doi.org/10.1007/s10965-006-0051-xAn

46) Hoti, G., Caldera, F., Cecone, C., Pedrazzo, A. R., Anceschi, A., Appleton, S. L., Monfared, Y. K. & Trotta, F. (2021). Effect of the Cross-Linking Density on the Swelling and Rheological Behavior of Ester-Bridged β-Cyclodextrin Nanosponges. Materials, 14(3), 478. https://doi.org/10.3390/ma14030478

47) Bujak, T., Nizioł-Łukaszewska, Z. & Wasilewski, T. (2018). Effect of Molecular Weight of Polymers on the Properties of Delicate Facial Foams. Tenside Surfactants Detergents, 55(2), 96–102. https://doi.org/10.3139/113.110547Figure

48) Yu, W. & Zhou, X. (2022). Experimental and modeling study of foam coarsening kinetics in porous media. Frontiers in Energy Research, 10. https://doi.org/10.3389/fenrg.2022.1012728

Appendix A

In Figure 28 a-c, the ^{1}H-NMR of P(AAm-co-4St), P(AAm-co-2St), and the polyacrylamide homopolymer is shown. In spectra a and b, distinct aromatic signals are observed. The signals are corresponding to the protons of the benzene ring of styrene (F). These signals are not present in the spectrum of the homopolymer, polyacrylamide (Figure 28C). This is confirming the absence of styrene in the homopolymer or in other words the presence of styrene in the copolymer P(AAm-co-St). Spectra shown in Figure 28 a and b also show signals in the aliphatic region. These are attributed to the methylene and methyl protons of the styrene moieties. These peaks however are absent or less pronounced in the spectrum of the homopolymer.

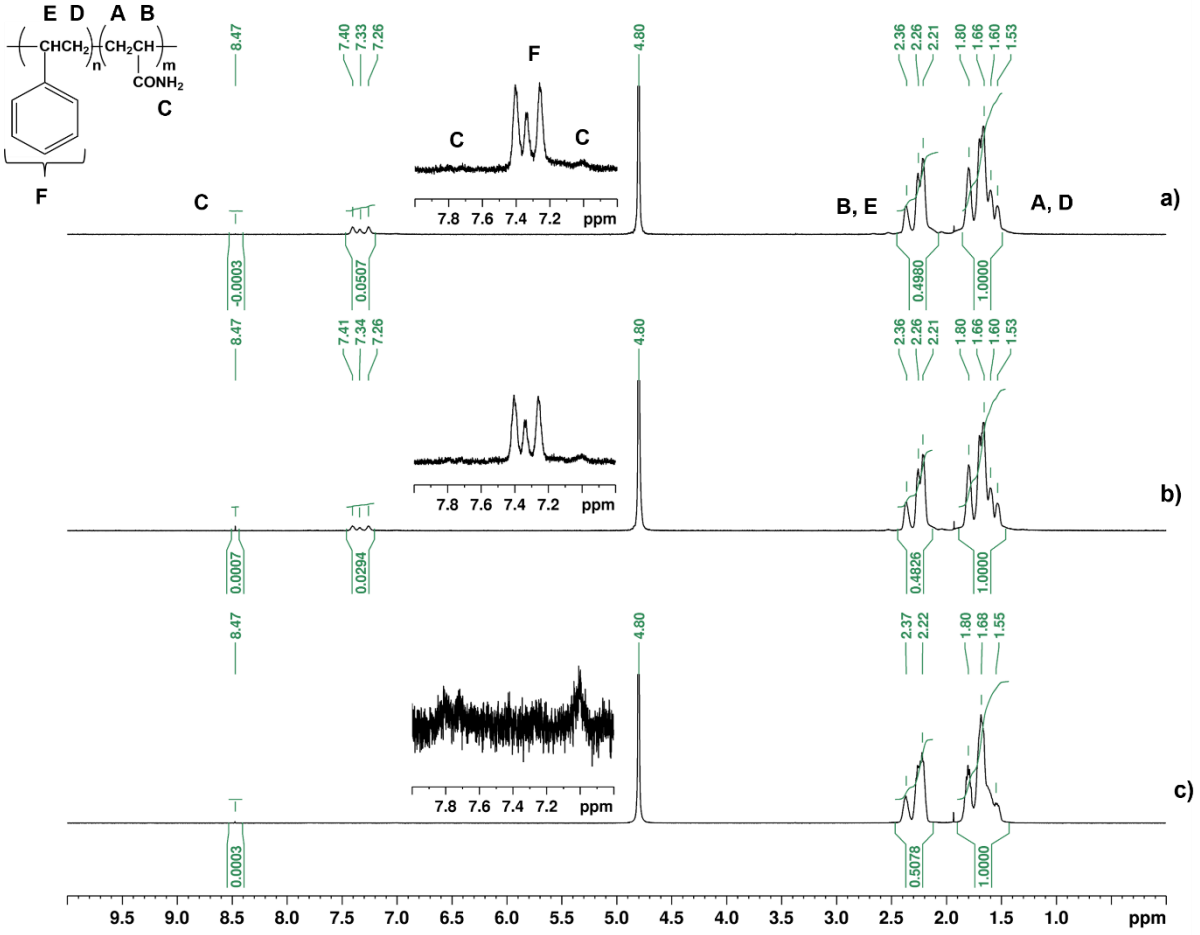

Figure 28 - ^{1}H-NMR spectrum of P(AAm-co-4St), P(AAm-co-2St), and polyacrylamide homopolymer, recorded in D2O.

Appendix B

Figure 29 shows the Foam of P(AAm-co-4St), which was derived from the ViEDRA. The foam was obtained by flushing the aqueous polymer/NaCl solution through the pipeline of the ViEDRA for ~150 cycles. Afterwards the foam was collected every 3-5 cycles.

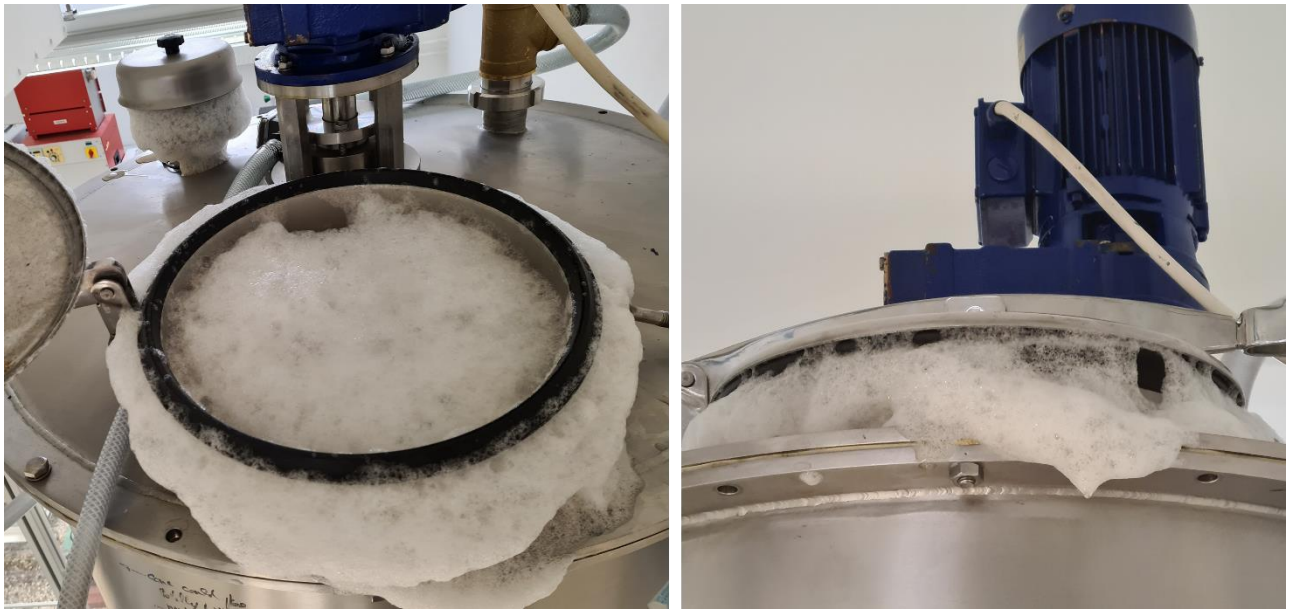

Figure 29 – Foam as it was recovered from the ViEDRA tank after flushing it through the pipeline ~150 times.

Appendix C

Table 7 presents the results of the elemental analysis of the as-synthesized P(AAm-co-4St). The objective of this experiment was to determine the quantity of CTAB that remained associated with the polymer following the synthesis. It was determined that 0.01 wt.% of Br was still associated with the polymer. This equals to an amount of 0.01 wt.% of CTAB. The Br amount of the purified polymer was found to be <0.01 wt %. This is indicating that CTAB was removed from the polymer due to precipitation and dialysis.

Table 7 - The composition of the as-synthesised P(AAm-co-4St), determined via elemental analysis.

	C (wt.%)	H (wt.%)	N (wt.%)	S (wt.%)	O (wt.%)	Br (wt.%)
as-synthesized P(AAm-co-4St)	48.20 ± 0.88	7.35 ± 0.01	18.09 ± 0.32	< 0.02	25.26 ± 0.62	0.01

Appendix D

The molecular weight of the PAAm homopolymer, P(AAm-co-2St) and P(AAm-co-4St) was determined by static light scattering in formamide.

Table 8 - Molecular weight in g/mol of PAAm homopolymer, P(AAm-co-2St) and P(AAm-co-4St) as determined by static light scattering in formamide

	PAAm	**P(AAm-co-2St)**	**P(AAm-co-4St)**
M_w [g/mol]	1110000±190000	590000±33000	370000±13000

English Abstract

The block copolymer P(AAm-co-St) was synthesized with varying amounts of styrene, and P(AAm-co-4St) was found to exhibit the most efficient stabilization of emulsions and the best foam-forming properties when compared directly. The interfacial tension between water and toluene was found to be significantly reduced by the as-synthesized polymer as well as by the purified polymer, with CTAB added after synthesis. PolyHIPEs and polyMIPEs were successfully synthesized using a comparatively low concentration of polymer. The resulting monoliths exhibited both, macro- and mesopores. The polyHIPEs exhibited a relatively high degree of porosity. In comparison, the polyMIPEs exhibited enhanced stiffness. Both variants had shown comparable swelling capacity and mechanical properties. Compared to the polyHIPEs from literature, the synthesized polyH/MIPEs had superior mechanical properties.[42] Additionally, P(AAm-co-4St) was found to produce foam in aqueous solution. Thereby, polymer was recovered from the solution in the ViEDRA. The results are promising for the fracking industry and may also be applicable to medical applications. However, further investigation is required to ascertain the potential issue of residual toxic acrylamide.

Deutsche Zusammenfassung

Im Rahmen der durchgeführten Experimente wurde das Blockcopolymer P(AAm-co-St) mit variierenden Anteilen an Styrol synthetisiert. Dabei konnte festgestellt werden, dass P(AAm-co-4St) im direkten Vergleich die Emulsionen am effizientesten stabilisiert und die besten schaumbildenden Eigenschaften aufweist. Es konnte nachgewiesen werden, dass die Grenzflächenspannung zwischen Wasser und Toluol sowohl durch das as-synthesized Polymer als auch durch das gereinigte Polymer mit zusätzlich hinzugefügtem CTAB signifikant reduziert wurde. Es konnte nachgewiesen werden, dass PolyHIPEs und PolyMIPEs mit einer vergleichsweise geringen Konzentration an Polymer erfolgreich hergestellt werden können. Die hergestellten Monolithe wiesen sowohl Makro- als auch Mesoporen auf. Im Falle der PolyHIPEs konnte eine hohe Porosität beobachtet werden. Die hergestellten PolyMIPEs wiesen eine erhöhte Steifigkeit auf. Hinsichtlich der Swelling Capacity sowie der mechanischen Eigenschaften zeigten beide Varianten vergleichbare Ergebnisse. Des Weiteren konnte P(AAm-co-4St) in wässriger Lösung geschäumt werden. In Versuchen mit dem ViEDRA konnte das Polymer als Schaum aus wässriger Lösung nach der Verwendung rückgewonnen werden. Die Ergebnisse sind vielversprechend für die Fracking-Industrie und potenziell auch für Anwendungen in der Medizin. Allerdings muss der Restgehalt an toxischem Acrylamid noch genauer untersucht werden.